Icarus 249 (2015) 108–128

Contents lists available at ScienceDirect

Icarus

journal homepage: www.elsevier.com/locate/icarus

# Gale crater and impact processes – Curiosity's first 364 Sols on Mars

Horton E. Newsom [a,*], Nicolas Mangold [b], Linda C. Kah [c], Joshua M. Williams [a], Ray E. Arvidson [d], Nathan Stein [d], Ann M. Ollila [a], John C. Bridges [e], Susanne P. Schwenzer [f], Penelope L. King [g,h], John A. Grant [i], Patrick Pinet [j], Nathan T. Bridges [k], Fred Calef III [l], Roger C. Wiens [m], John G. Spray [n], David T. Vaniman [o], Wolf E. Elston [a], Jeff A. Berger [p], James B. Garvin [q], Marisa C. Palucis [r], the MSL Science Team

[a] Institute of Meteoritics, Department of Earth and Planetary Sciences, Albuquerque, NM 87131, USA
[b] LPGN, CNRS, UMR 6112, Université Nantes, Nantes, France
[c] Department of Earth and Planetary Sciences, University of Tennessee, Knoxville, TN 37996, USA
[d] Washington University in Saint Louis, Saint Louis, MO, USA
[e] Space Research Centre, Dept. of Physics and Astronomy, University of Leicester, Leicester, LE1 7RH, UK
[f] Department of Physical Science, The Open University, Walton Hall, Milton Keynes MK7 6AA, UK
[g] Research School of Earth Sciences, Australian National University, Canberra, Australia
[h] University of Guelph, Guelph, Ontario, Canada
[i] Center for Earth and Planetary Studies, National Air and Space Museum, Smithsonian Institution, Washington, DC 20560, USA
[j] Université Paul Sabatier, Institut de Recherche en Astrophysique et Planétologie (IRAP), Toulouse, France
[k] Applied Physics Laboratory, Laurel, MD 20723, USA
[l] Jet Propulsion Laboratory, California Institute of Technology, Pasadena, CA 91109, USA
[m] Los Alamos National Laboratory, Los Alamos, NM 87545, USA
[n] Planetary and Space Science Centre, University of New Brunswick, Fredericton, NB E3B 5A3, Canada
[o] Planetary Science Institute, Tucson, AZ 85719, USA
[p] University of Western Ontario, London, Ontario, Canada
[q] NASA Goddard Space Flight Center, Greenbelt, MD 20771, USA
[r] Department of Earth and Planetary Science, University of California at Berkeley, Berkeley, CA 94720, USA

ARTICLE INFO

*Article history:*
Received 31 January 2014
Revised 1 October 2014
Accepted 2 October 2014
Available online 1 November 2014

*Keywords:*
Mars, surface
Impact processes
Cratering

ABSTRACT

Impact processes at all scales have been involved in the formation and subsequent evolution of Gale crater. Small impact craters in the vicinity of the Curiosity MSL landing site and rover traverse during the 364 Sols after landing have been studied both from orbit and the surface. Evidence for the effect of impacts on basement outcrops may include loose blocks of sandstone and conglomerate, and disrupted (fractured) sedimentary layers, which are not obviously displaced by erosion. Impact ejecta blankets are likely to be present, but in the absence of distinct glass or impact melt phases are difficult to distinguish from sedimentary/volcaniclastic breccia and conglomerate deposits. The occurrence of individual blocks with diverse petrological characteristics, including igneous textures, have been identified across the surface of Bradbury Rise, and some of these blocks may represent distal ejecta from larger craters in the vicinity of Gale. Distal ejecta may also occur in the form of impact spherules identified in the sediments and drift material. Possible examples of impactites in the form of shatter cones, shocked rocks, and ropy textured fragments of materials that may have been molten have been observed, but cannot be uniquely confirmed. Modification by aeolian processes of craters smaller than 40 m in diameter observed in this study, are indicated by erosion of crater rims, and infill of craters with aeolian and airfall dust deposits. Estimates for resurfacing suggest that craters less than 15 m in diameter may represent steady state between production and destruction. The smallest candidate impact crater observed is ~0.6 m in diameter. The observed crater record and other data are consistent with a resurfacing rate of the order of 10 mm/Myr; considerably greater than the rate from impact cratering alone, but remarkably lower than terrestrial erosion rates.



* Corresponding author.

http://dx.doi.org/10.1016/j.icarus.2014.10.013
0019-1035/

## 1. Introduction

The surface of Mars has been affected by impact cratering processes throughout its history. Gale crater is an example of an impact crater (155 km diameter) that formed in the late Noachian to early Hesperian (Anderson and Bell, 2010; Thomson et al., 2011), most likely as complex crater (Pike, 1980; Schwenzer et al., 2012). Gale crater and vicinity comprise a rich and diverse geologic history, including volcanic activity (Stolper et al., 2013; Schmidt et al., 2013), mineralogical evidence for aqueous alteration (Milliken et al., 2010; Fraeman et al., 2013; Ehlmann and Buz, 2014), and the presence of fluvial and lacustrine sedimentary environments (Williams et al., 2013; Grotzinger et al., 2013; Palucis et al., 2014). The early results from the MSL mission provide evidence for a habitable environment with abundant near-neutral pH water (Grotzinger et al., 2013). Understanding the effects of impact cratering on surficial materials provides insight into how later, smaller impacts and subsequent aeolian processes may complicate the interpretation of the preserved stratigraphic record, as well as provide constraints on resurfacing rates.

Gale crater is superimposed on the martian dichotomy boundary and, more specifically, formed on Noachian and Hesperian-aged units on its eastern, southern and western margins. Gale is bounded by Noachian to Amazonian aged transitional materials on its northern margins according to the new *Geologic Map of Mars* (Tanaka et al., 2014a,b). A schematic map (Fig. 1B) provides the context for this study, as well as highlighting Gale crater ejecta that were not well identified in past studies. The mapping was done at a regional scale using the THEMIS daytime and nighttime mosaic. Thermal imagery is especially powerful to differentiate patterns related to the crater's ejecta, which behave differently than surrounding bedrock. HRSC, CTX and HiRISE images were used to locally check the mapping, but coverage was partial and was not used for the full scale mapping.

Orbital images show thick ejecta outside of Gale's rim, particularly around the southern rim, indicating that it is one of the younger large craters in the region. Superimposed on the Gale deposits are five craters mapped with fresh ejecta blankets (Fig. 1B). Distal ejecta from these nearby, similarly aged or younger craters are likely to have diverse compositions reflecting the varied lithology of martian crust north and south of the dichotomy. Variations in the regional chemistry have been noted, for example, in Odyssey Gamma Ray data (Newsom et al., 2013a,b). There is a strong potential for some of the ejecta from these more recent craters to have formed secondary craters and be present as loose blocks within Gale crater.

The original morphometry of Gale has also been extensively modified by accumulation of deposits preserved within the central mound, Aeolis Mons (informally named Mt. Sharp), which can include sedimentary and/or volcaniclastic and distal ejecta deposits. In addition, the crater contains alluvial and fluvial deposits originating at the crater rim, and younger (i.e., active) sedimentary dunes and dust deposits (Silvestro et al., 2012). Crater count studies by Grant et al. (2014) show that the bulk of the alluvial deposits of Gale were deposited in the Hesperian, in particular the Peace Vallis Fan, including the distal Bright Fractured terrain, that includes Yellowknife Bay studied by Curiosity, date to 3.2–3.3 Ga. The thick succession of strata preserved within Mt. Sharp could represent an erosional remnant of a much more extensive crater fill (Cabrol et al., 1999; Malin and Edgett, 2000), or reflect its original shape resulting from atmospheric effects during mound growth (Kite et al., 2013). Much of the rest of the crater floor, including the

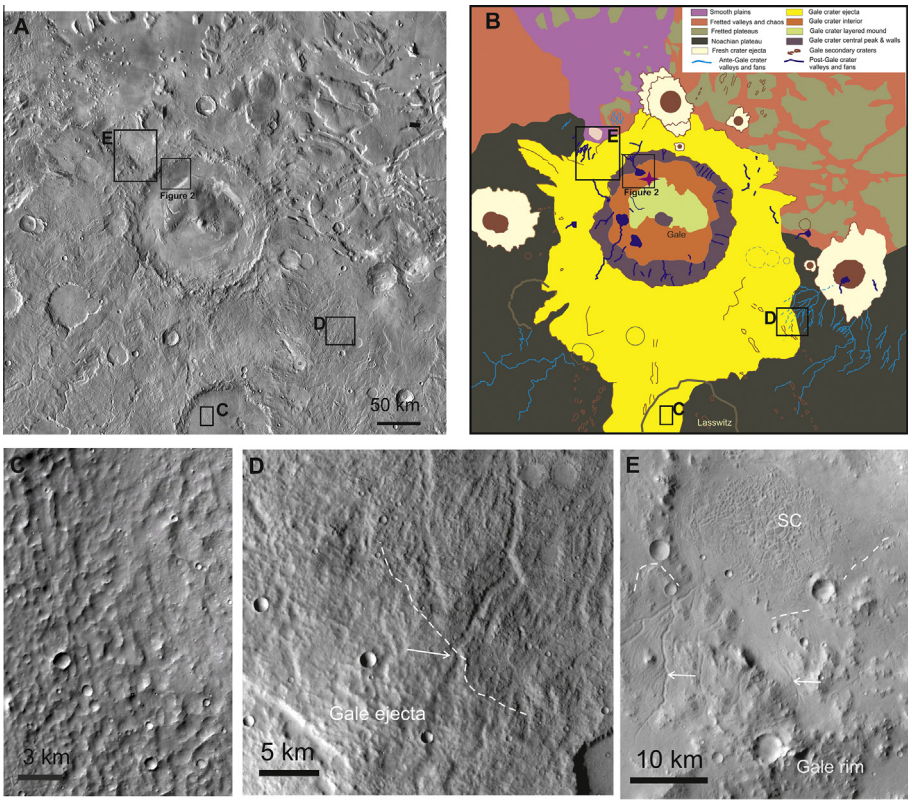


**Fig. 1.** (A) THEMIS mosaic of Gale crater and surroundings (http://www.mars.asu.edu/data/thm_dir/). (B) Geological sketch map of the same area. The star in the box labeled "Fig. 2" denotes the landing site of Curiosity. (C) Hummocky terrain typical of thick ejecta deposits. Portion of CTX image B21_017720_1703. (D) The dashed white line separates approximately hummocky material interpreted as ejecta to the left from non-buried highlands to the right. The white arrow points to a fluvial valley apparently buried beneath ejecta. Portion of HRSC image from orbit 5273. (E) Examples of fluvial valleys incising ejecta are indicated by white arrows. SC indicates small chaotic terrains on the floor of Gale. Portion of HRSC image, orbit 4191.

Bradbury Landing site of MSL, and possibly the lower portions of Mt. Sharp, are buried by sediment inferred to have originated at the crater rim, such as the surficial deposits that comprise the Peace Vallis fan (Palucis et al., 2014), the fine-grained lacustrine strata of the Yellowknife Bay formation (Grotzinger et al., 2013), and, probably, the fluvial conglomerates on Bradbury Rise (Williams et al., 2013). The possible derivation of some of the sediments from the central uplift and/or Mt. Sharp cannot be ruled out, however (Dietrich et al., 2014).

This work provides an overview of small (simple) impact craters and related materials observed within Gale crater, both from orbit and from the Curiosity rover during the first 364 Sols of the MSL mission. During this time the rover initially studied the materials near the landing site on Bradbury Rise (Sols 0–123), including a stop at the Rocknest drift deposit (Sols 55–102). The rover then explored the bright fractured units of Yellowknife Bay (Sols 124–299), including extensive time in the vicinity of the drill sites at John Klein (Sols 163–198) and Cumberland (Sols 272–292). After departing Yellowknife Bay, the rover returned to the Hummocky Plains units from Sol 300 to Sol 364 (the limit for discussion of most of the features described in this paper). This record of cratering combined with other data provides constraints on the erosional history of the area investigated by Curiosity.

## 2. Image surveys – sources and analysis methods

### 2.1. Crater measurements from orbital data

The Mars Reconnaissance Orbiter (MRO) contains two imagers used for orbital evaluation of Gale crater. The HiRISE instrument (McEwen et al., 2007) provides the highest resolution images (25 cm per pixel), which was also used to create a Digital Elevation Model (DEM) (1 m per pixel elevation) (Golombek et al., 2012; Kirk et al., 2011). The CTX camera (Malin et al., 2007) provides ~6 m resolution gray scale images with broader coverage than the HiRISE images, and was used for some of the mapping.

### 2.2. Surveys near the rover of small craters, the abundance and nature of isolated blocks

The NavCam and other engineering cameras provide the most comprehensive view of the areas around the rover (Maki et al., 2011). The vertically projected NavCam mosaics produced by the MSL Operational Product Generation Subsystem (OPGS) group (Helen Mortensen lead) provided essential data to examine isolated blocks and small crater forms at the decimeter to meter scale to evaluate their circularity. The stereo NavCam data allowed examination of candidate craters for existence of a central depression. A confirmed crater has a minimum/maximum diameter ratio greater than 70% based on the topographic rim and distribution of ejecta blocks. During the rover traverse, numerous blocks of float were encountered on top of bedrock or regolith. To better understand the areal abundance of these larger blocks, a survey was conducted of the number of blocks (>20 cm in length) visible in the NavCam mosaics around the stops on Bradbury Rise up to Sol 361 to a distance of 18 m from the rover as described below (Table 1). The area visible in the projected NavCam mosaics was calculated and corrected for the areas obscured by the Rover itself, especially the area to the rear.

**Table 1**
Float rocks > 20 cm visible in vertically projected NavCam mosaics provided by the MSL mission. In some Sols the NavCam survey did not cover a full 360°. The last column is the abundance of blocks per 100 $m^2$, approximately the area in the ChemCam targetable area around the rover out to ~5.6 m. Examples of the mosaics used to obtain this data are available by Sol number at: http://mars.jpl.nasa.gov/msl/multimedia/mosaics.

| Sol | N | Area ($m^2$) | N/$m^2$ | N/100 $m^2$ |
|---|---|---|---|---|
| 2 | 1 | 150 | 0.007 | 0.67 |
| 22 | 7 | 150 | 0.047 | 4.7 |
| 24 | 2 | 150 | 0.013 | 1.3 |
| 26 | 2 | 150 | 0.013 | 1.3 |
| 29 | 4 | 150 | 0.027 | 2.7 |
| 38 | 5 | 150 | 0.033 | 3.3 |
| 39 | 0 | 55 | 0.000 | 0.00 |
| 40 | 1 | 150 | 0.007 | 0.67 |
| 41 | 1 | 40 | 0.025 | 2.5 |
| 42 | 2 | 40 | 0.050 | 5.0 |
| 43 | 3 | 150 | 0.020 | 2.0 |
| 48 | 1 | 150 | 0.007 | 0.67 |
| 336 | 2 | 150 | 0.013 | 1.3 |
| 337 | 2 | 80 | 0.025 | 2.5 |
| 338 | 0 | 150 | 0.000 | 0.00 |
| 340 | 16 | 150 | 0.11 | 11 |
| 342 | 3 | 150 | 0.020 | 2.0 |
| 343 | 2 | 150 | 0.013 | 1.3 |
| 344 | 7 | 150 | 0.047 | 4.7 |
| 345 | 3 | 150 | 0.020 | 2.00 |
| 347 | 6 | 64 | 0.094 | 9.4 |
| 349 | 4 | 150 | 0.027 | 2.7 |
| 351 | 3 | 150 | 0.020 | 2.0 |
| 354 | 1 | 150 | 0.007 | 0.7 |
| 356 | 3 | 150 | 0.020 | 2.0 |
| All | 81 | 3279 | 0.025 | 2.5 |
| −340 | 65 | 3129 | 0.021 | 2.1 |

### 2.3. Estimation of dip

The dip of blocks that might have been dislodged by impacts was estimated semi-quantitatively from stereo images from the rover. A combination of Mastcam and NavCam images allowed the dip of the blocks to be determined from their orientation and angle to the horizontal, in addition to the angle down from the cameras to the sample, which can be determined with the MSLICE software used by the project. Uncertainty depends on the orientation of the blocks but is usually less than or equal to 10°.

### 2.4. Impactite and spherule survey

A search for possible impactites, including shatter cones, impact melts and disrupted bedrock was conducted primarily using color images from the narrow M100 and wide angle M34 color mast cameras (Mastcam) (Malin et al., 2010). This imagery included occasional 360° surveys and the more frequent Mastcam images of the workspace in front of the rover, targets of opportunity images selected by the daily operations groups, and documentation images of the ChemCam blind targets. Resolution and image coverage limited the impactite survey to the area within ~6 m of the rover. The NavCam panchromatic images were less useful for this purpose because of their lower resolution. Other images from The Mars Descent Imager (MARDI) and Hazcam were examined but were very limited in areal extent for the first 360 Sols. High resolution images of impactite materials were also obtained with the mast mounted Remote Micro Imager (RMI), which is part of the ChemCam instrument (Maurice et al., 2012; Le Mouélic et al., 2015). The Mars Hand Lens Imager (MAHLI) on the rover arm (Edgett et al., 2012) provides high-resolution (~15–30 μm per pixel) color images of materials close to the rover, and this was used to image candidate impact spherules in the trenches and rover tracks, on rock outcrops and material dumped on the observation plate. A z-stack technique is used to combine the best focused portions of multiple images taken at different focus settings to increase the depth of field.

## 3. Gale crater setting and formation

Gale crater (sketch map for context seen in Fig. 1B) is located predominantly within highlands crust. The interior of Gale contains fluvial valleys, sedimentary deposits, and a possible central peak exposed on the south side of Mt. Sharp. Gale ejecta were mapped based on the identification of hummocky patterns (Fig. 1C), and lobate forms typical of ejecta deposits (Fig. 1B). The mapped boundaries are commonly indicated by dashed lines because the limit is not always easy to follow because erosional degradation has modified the boundary, or because of limited high resolution image coverage (Fig. 1D). Beyond the edge of the annulus containing the continuous ejecta blanket, discontinuous ejecta are preserved as rays and secondary ejecta mapped as brown curvilinear features in Fig. 1B. Crosscutting relationships show that Gale ejecta are superimposed on dissected highlands of the Noachian period (Tanaka et al., 2014a,b), as well as on several Noachian-age craters, for instance Lasswitz crater to the south, which display low depth–diameter ratio and strongly eroded rims typical of Noachian craters (e.g. Mangold et al. (2012b)). The relationships are more complicated to the north where the occurrence, or preservation, of ejecta seems more limited. Local rays of Gale ejecta are found on the plateaus of chaotic terrains (Meresse et al., 2008; Chapman and Tanaka, 2002) (Fig. 1B), but material from the fretted valleys (which are bounded by these plateaus) and the smooth plains to the north-west is distinct from ejecta and is likely superimposed over Gale crater ejecta. The ages were determined by crater counts on the southern ejecta blanket by Thomson et al. (2011), Bustard et al. (2012) and Le Deit et al. (2013) are ~3.7 Gy (see Michael and Neukum (2010) and Michael (2013) for current methodology). This age is also consistent with the Ar–Ar dating (4.16 ± 0.4 Gy) of the crust formation age of materials now in Yellowknife Bay (Farley et al., 2013), regional stratigraphic relationships, including the Late Hesperian–Early Amazonian resurfacing of northern terrains and formation of fretted valleys.

Superposition relationships between regional fluvial landforms and later Gale crater have also been mapped. The cratered highlands fluvial networks are interpreted as part of the Late Noachian–Early Hesperian period of fluvial activity (e.g., Fassett and Head, 2008). These widespread valleys are locally buried beneath Gale ejecta (Fig. 1A, in blue[1] in Fig. 1B and D). By contrast, the valleys inside Gale are limited to small watersheds on the rim and Mt. Sharp, and do not extend beyond the Gale ejecta. A few valleys cut the Gale crater rim (Fig. 1A and D, in blue in Fig. 1B), including Peace Vallis, upstream of the Curiosity landing site (Williams et al., 2013). Locally, other valleys cut through ejecta, such as northeast of Peace Vallis, where valleys form a 40 km wide watershed and join a depression with small chaotic terrains that also post-date ejecta (Fig. 1E). These relationships imply that Gale crater formed either close to the end of the main period of fluvial activity in the Noachian to Early Hesperian (e.g., Fassett and Head, 2008), or between the end of this main period of activity and the Late Hesperian (~3.4–2.9 Gy) episode of fluvial activity found in several regions on Mars (e.g., Mangold et al., 2004, 2012a,b; Quantin et al., 2005; Grant and Wilson, 2011). An impact age of Late Noachian to Early Hesperian suggests both hypotheses are possible for the age of these valleys. Nevertheless, several observations point toward late stage activity for the valleys found inside Gale crater (Anderson and Bell, 2010). First, ejecta remain largely undissected by fluvial valleys, suggesting later fluvial activity was localized and not as widespread as with the Noachian valleys. Second, is the presence of late-stage valleys outside of the ejecta blanket that cross post-Noachian terrains (in purple, to the east on Fig. 1B). Lastly, crater counts on Peace Vallis fan showing Late Hesperian to Early Amazonian ages (Grant et al., 2014) demonstrate that post-Noachian fluvial activities occurred. In this chronology, Gale crater shares characteristics with Holden crater, where post-Noachian valleys also incise ejecta (Mangold et al., 2012a).

[1] For interpretation of color in Fig. 1, the reader is referred to the web version of this article.

## 4. Impact crater frequency and depth–diameter ratios

The Hummocky Plains (HP) and Bright Fractured (BF) surfaces that have been directly visited by Curiosity are found on the Gale crater interior units and form part of the family of large areas with ages from craters >400 m in diameter indicating the surface formed <3.2–3.3 Ga from the study of Grant et al. (2014) as summarized above in the Introduction. A limited area near the Curiosity landing site was examined to determine the preservation state of the craters and their relative frequency (Location Fig. 2B). The area studied contained too few craters to determine useful ages. Craters of various sizes were identified and depths retrieved using co-registered HiRISE and HiRISE-derived DEM data. Examination of HiRISE data covering the HP and BF surfaces show a range of crater preservation states, with a few pristine-looking craters and numerous craters that appear shallow and degraded (Fig. 3). Every feature seen at full HiRISE resolution in stereo images that had a circular profile and a distinct depression was counted and measured. The DEM allow depth determinations on the order of 20 cm under ideal conditions (e.g. Kirk et al., 2008). As described below in the next section on observation of small craters from the rover, the Hummocky Plains contains abundant topographic features on the 3–10 m scale, that appear to be possible craters in low resolution images, such as Fig. 3, but which do not meet the criteria of being confirmed craters due to non-circular shape or lack of a depression.

The cumulative crater abundances versus diameter (Fig. 4) were determined for the relatively small crater sizes (<100 m diameter) within a few hundred meters of the Bradbury Landing site and areas traversed within the first 360 Sols. The crater population drops off at smaller sizes from an expected log linear production function curve as shown, beginning at diameters of 10–15 m, down to the smallest craters measured at 2.75 m. The reduced number of these small craters is consistent with observations from Curiosity's NavCam and Mastcam imaging systems showing that shallow craters are being erased by surface processes. These processes include infilling by aeolian deposits, as well as the ongoing aeolian erosion of the crater rims, which affect small craters the most (see below). Craters in the size range from 3 to 15 m diameter are easily resolvable in the HiRISE images and only for craters at the very smallest size bin could the drop off include some issues with resolution, as discussed below.

The maximum extent of vertical reworking of the surface and shallow subsurface can be assessed by assuming that all craters start with the same depths as seemingly fresh craters. Kenkmann et al. (2013) indicates that fresh simple craters have a depth–diameter ratio of ~0.2 (a range of 0.14–0.28 is cited). The crater depth–diameter data (Fig. 5) was measured for regions that include both HP and BF surfaces. Crater diameters and depths were measured using co-registered HiRISE and HiRISE-derived DEM data. From the data, craters smaller than 10–15 m in diameter exhibit a wide range of depths from deep to very shallow and presumably nearly completely filled, consistent with the expectation that small craters will be more rapidly eroded. A crater 15 m in diameter will be erased by erosion of 1.5–3 m. Craters greater than 15 m in diameter converge to an average depth diameter ratio less than 0.1, suggesting either a shallower original depth, the presence of substantial fill, or simply the absence of really fresh craters greater

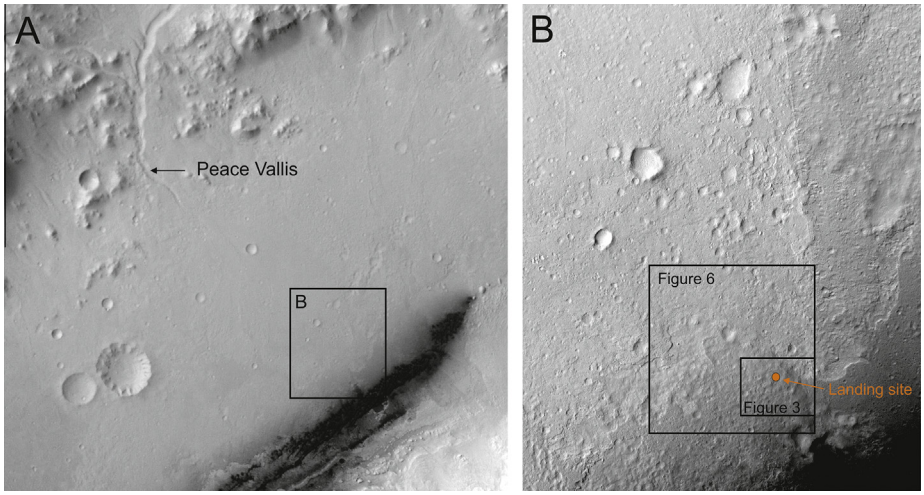


**Fig. 2.** Context images. (A) HRSC image (orbit number #5273) of the overall landing site area with Peace Vallis visible on the top left corner. (B) HiRISE images PSP_010639_1755_RED and PSP_009571_1755_RED of the landing area south of the Peace Vallis fan containing the location of the landing site and areas for Figs. 4 and 7.

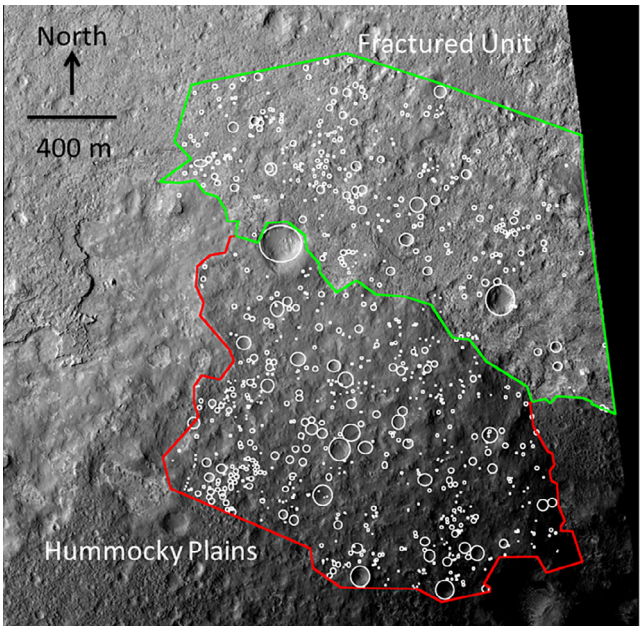


**Fig. 3.** Location of craters identified and measured for depth and diameter from HiRISE images of the area near the landing site of MSL and MSL operations during the first 360 Sols. Red star denotes the landing site. Image: NASA/JPL-Caltech/University of Arizona, PSP_010639_1755. (For interpretation of the references to color in this figure legend, the reader is referred to the web version of this article.)

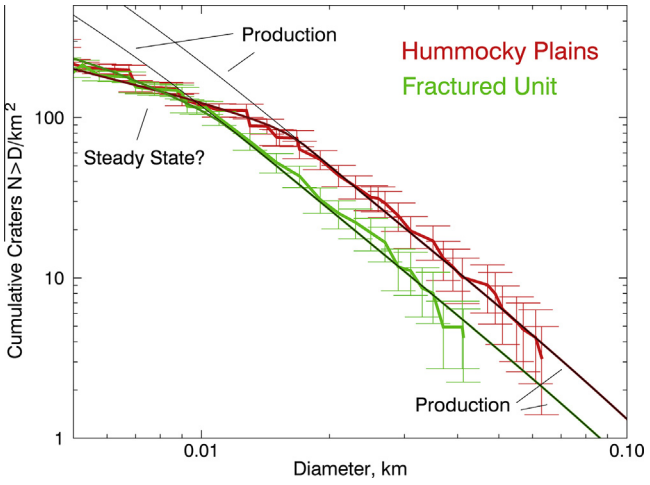


**Fig. 4.** Plot of cumulative impact crater abundance versus diameter for the Hummocky Plains and Bright Fractured (BF) Unit for craters identified in Fig. 3. Two different crater production curves are shown as discussed in the text. At diameters less than ~10–15 m the down turn in cumulative craters may reflect a combination of crater degradation and production that may reflect a steady state crater population.

than 15 m in diameter in the small sampled area because they form less frequently. One possible source of scatter in the depth diameter data is enlargement of craters by erosion, but this is unlikely in the areas investigated. As discussed in the following section, the crater diameters are minimally affected as they degrade because the dominant resurfacing processes seem to be aeolian infill and erosion of the higher projecting portions of the crater rim, which reduces the depth, but is unlikely to change the crater diameter significantly for craters less than the 90 m diameter craters studied here. Elsewhere on Mars, the steep interior walls of larger craters that are not rapidly filled by sediments, such as Endurance Crater at Meridiani Planum, Mars (Watters et al., 2011), can be eroded by sand abrasion, with rim enlargement that results in a shallower depth diameter ratio. On the Earth, rainfall is more effective at eroding the steep interior slopes of even small craters leading to crater rim enlargement (Kumar et al., 2010).

Compared to the well-known slope of the crater production function (Hartmann and Neukum, 2001), the crater size frequency distributions for the data turn over for crater sizes less than ~10–15 m, which is consistent with slow, steady removal of smaller craters. The resurfacing rate (i.e., removing craters by erosion of rims and infilling of interiors) must be greater than 3–5 m over several billion years, in order to remove many of the craters less than 10–15 m in diameter in the time interval since the last episodes of fluvial activity in Gale (Grant et al., 2014). The origin of the slightly lower value of the cumulative crater abundances for the BF as opposed to the HP (Fig. 4) is unknown, but could be due to a slightly more recent exhumation of the BF, or more rapid erosion of craters in the BF.

## 5. Small craters and impact effects

The area traversed by the MSL rover Curiosity during the first year of operation (Fig. 6) contains numerous impact craters ranging in diameter from over 100 m, down to as small as 0.6 m.

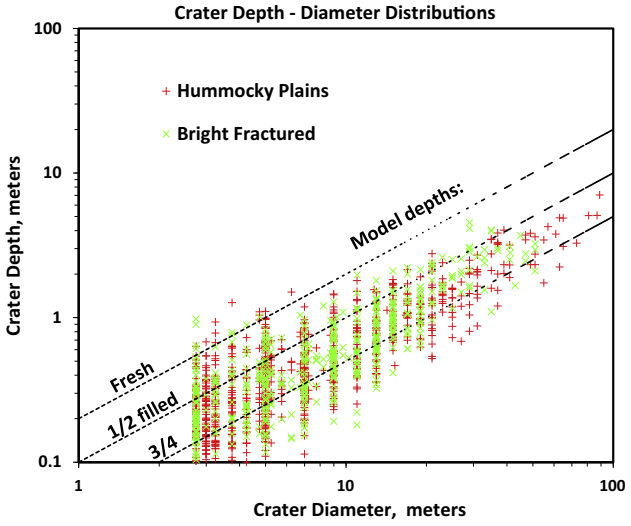


**Fig. 5.** Plot of impact crater depth and diameter data for the Hummocky Plains and Light Toned Fractured Unit, for craters identified in Fig. 4. A line showing the expected relationship for fresh craters is based on a crater depth ~0.2 times the crater diameters (Kenkmann et al., 2013). Lines for partially filled craters with $d/D = 0.1$ (half filled) and $d/D = 0.05$ (3/4 filled) are also shown. Although actual crater depths will be somewhat variable, there is a clear indication that many craters less than 40 m in diameter are substantially reduced in depth due to rim erosion and infill as observed from the rover.

The criteria for identification of the smallest craters are described in the methods section. Curiosity's traverse includes several geomorphic regions (Fig. 7) with distinct impact crater signatures, including the Hummocky Plains (HP) unit, the Glenelg Member, which is a slope partly covered in regolith traversed after Sol 50 on the way down to the contact with the Bright Fractured (BF) unit of Yellowknife Bay, and a low albedo, Cratered Surface (CS) (Grotzinger et al., 2013). The most aerially extensive region visited during the first year is the HP unit, which contains many distinct crater forms. The BF unit of Yellowknife Bay has the lowest abundance of craters. The CS preserves the highest concentration of craters, but was not visited by Curiosity. By contrast, the slope down to Yellowknife Bay traversed by the rover has a somewhat larger local concentration of overlapping crater forms (Fig. 7). The variable concentrations of craters on different units could be due to stochastic variations in the impact locations, variable rates of deposition of the sediments and variable rates of later erosion and exhumation. Variable abundances and distributions of secondary craters could also explain some of the differences in the crater distributions in Figs. 6 and 7. As seen around Zunil crater secondary craters are distinctive asymmetrical in shape with sharp rims and bright ejecta and rays (McEwen et al., 2005). However, the craters observed from Curiosity are relatively circular, and are probably not secondaries, but this possibility cannot be ruled out for all craters.

Several examples of craters that are located near the rover traverse, which were imaged with the Mast Cameras (Fig. 8) are described here. Crater 1 (Fig. 8A) is located near the landing zone on Bradbury Rise (see Figs. 6 and 7 for location). It is a small degraded crater with a diameter of 3.4 m. The crater rim is lined with angular to subangular clasts ranging in size from 1.0 to 8.0 cm. The central portion of the crater interior is lacking the larger clasts seen outside the crater, but the finer-grain portion seems otherwise similar to the material outside the crater in the

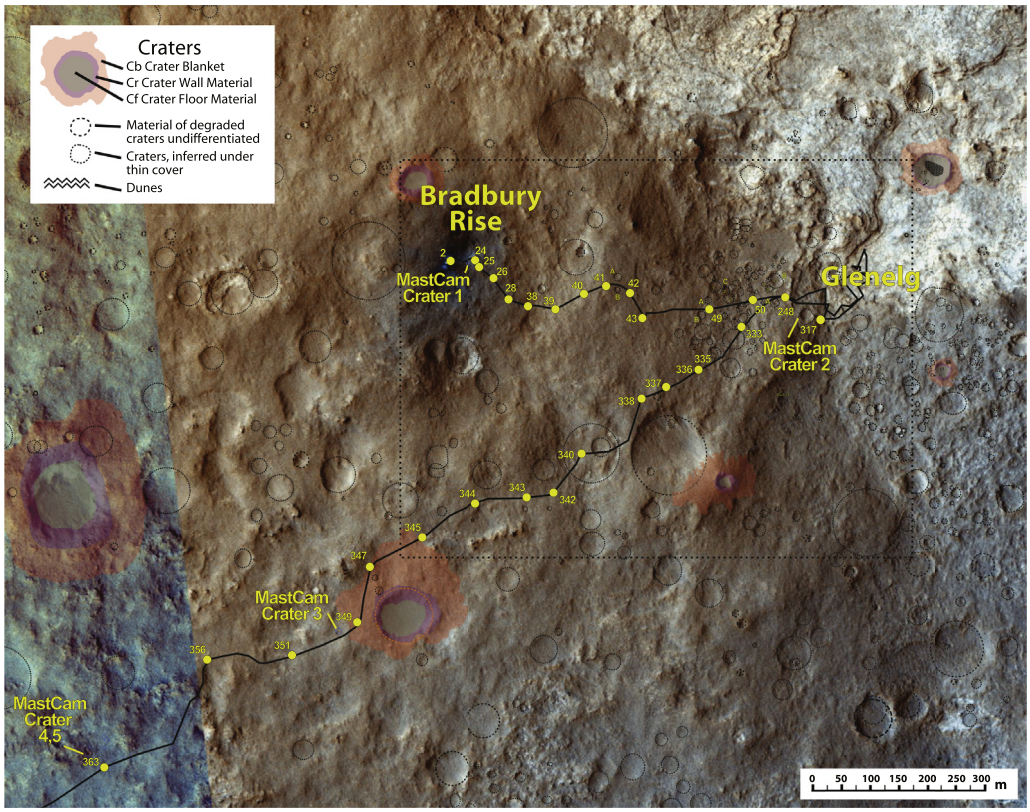


**Fig. 6.** MastCam crater reference map. Rover traverse path and rover stops by Sol number up to Sol 363 are plotted on a HiRISE image base. The Bradbury Rise area where the Rover landed is located on Hummocky Unit material (Fig. 7). The Glenelg area was the first destination for the Rover. This map labels four areas with one or two craters imaged by MastCam. Several of the freshest craters included mappable ejecta blankets, rims and floors. Image: NASA/JPL-Caltech/University of Arizona.

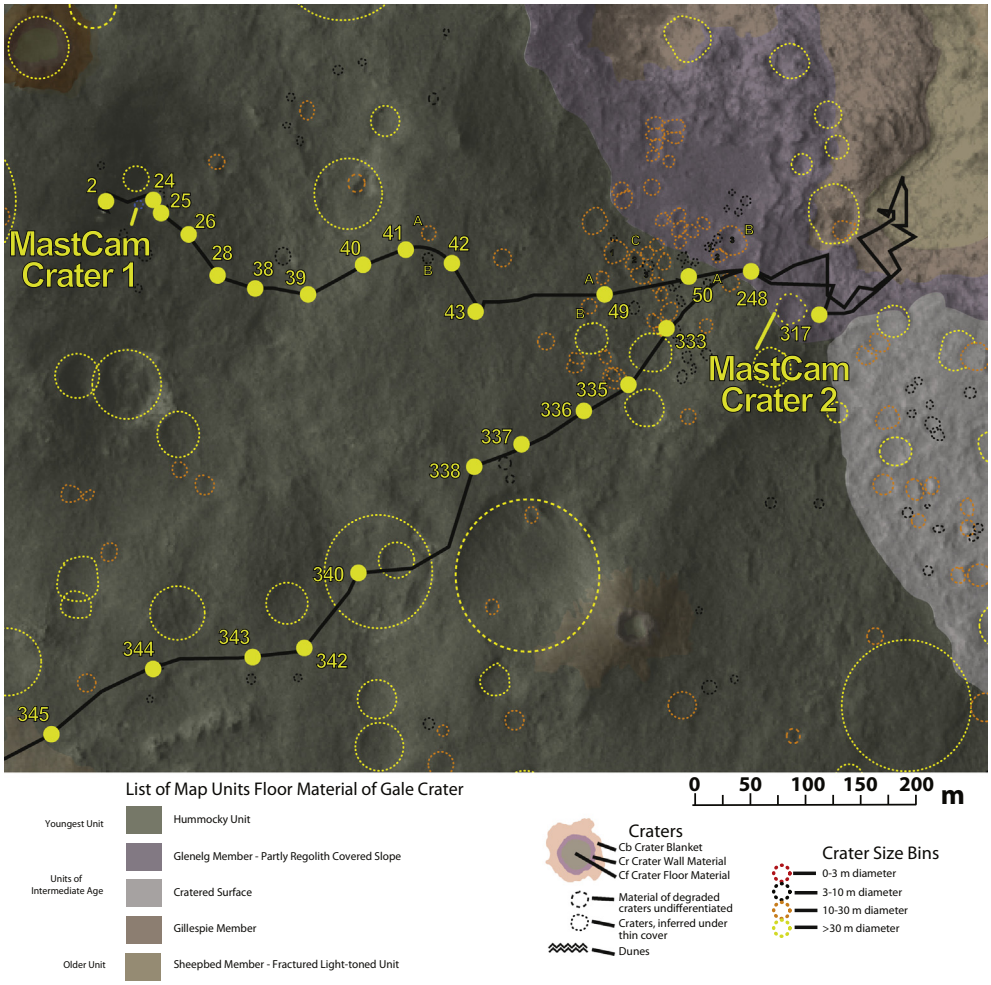


**Fig. 7.** Rover traverse path and stops with geology plotted on a HiRISE image base, after Grotzinger et al. (2013). This map depicts a closer view of two of the four sites imaged by MastCam that were used in this study. The map also shows the four different units for the floor material in the Glenelg/Bradbury Rise area. NASA/JPL-Caltech/University of Arizona.

image. Accumulation of fine-grained drift material or dust deposits is not evident, presumably because of the shallow nature of the feature. Crater 2 (Fig. 8B), located on the edge of the Hummocky terrain, was originally imaged by MastCam on Sol 54 as a possible candidate for scooping and contact science. The crater is 20 m in diameter and is generally less degraded than Crater 1. The rim of Crater 2 is lined with large clasts ranging from 0.1 to 1.0 m in size. The clasts are heterogeneous and appear to originate from two different types of parent rock. The clasts toward the east (far side of Fig. 8B) are light toned and layered, whereas the clasts toward the west (near side of Fig. 8B) are dark toned and not layered. The floor of the crater is filled with fine-grained regolith interspersed with a few small blocks up to ~8 cm across. Crater 3 (Fig. 8C) is located in the hummocky unit further to the west (see Fig. 7 for context) and imaged with Left and Right MastCam on Sol 351. This crater is circular in stereo HiRISE images (e.g. ESP_028335_1755_ESP_028269_1755/ESP_028335_1755_ESP_028269_1755_RED), and is deeper and less filled-in than Craters 1 and 2, based on qualitative evaluation of stereo Navcam imagery. The crater rim is lined with loose blocks (not outcrops of bedrock) ranging from 0.1 to 0.75 m in size, with the characteristic variable clast size texture of conglomerate (Figs. 8C and 9B). A few smaller light-toned fine-grained blocks are present on the near rim on the right side. The interior of the crater is filled with regolith that lacks the abundant variable size clasts of the regolith outside of the crater, and includes some outcrops or blocks of conglomerate (Fig. 9B). The two craters 4 and 5 (imaged on Sol 364, Fig. 8D) are located further southwest on the traverse from Crater 3. Craters 4 and 5 are the deepest of the five craters, and based on Fig. 8D the inside of the crater on the left side and the central crater floor are filled with a fine-grain regolith similar in appearance to the surfaces external to the crater, but without any larger clasts. The right side of the crater interior and part of the floor appear to contain numerous larger clasts of different sizes. The craters are less circular with Crater 4 having a 70% ratio of the short diameter of the long diameter, but the craters are located on the side of a low rise. The rim of the closer Crater 4 is lined with large blocks ranging from 0.1 to 0.25 m in size (Fig. 8D). Almost all of the rim clasts have the texture of conglomerates (Fig. 8D). The interior of the northeast rim appears covered with a fine layer of dust that could be associated with modern aeolian processes.

Ongoing degradation of small craters along Curiosity's traverse primarily reflects aeolian activity. The freshest (and possibly youngest) craters have blocky rims and have deposits of bright fine-grained aeolian materials on their relatively deeper floors. With increasing degradation, the craters seem to experience removal of the rim blocks, presumably due to aeolian processes. When sand is mobilized it can also locally abrade rocks and ventifacts are common (Bridges et al., 2014). The role of abrasion on protruding

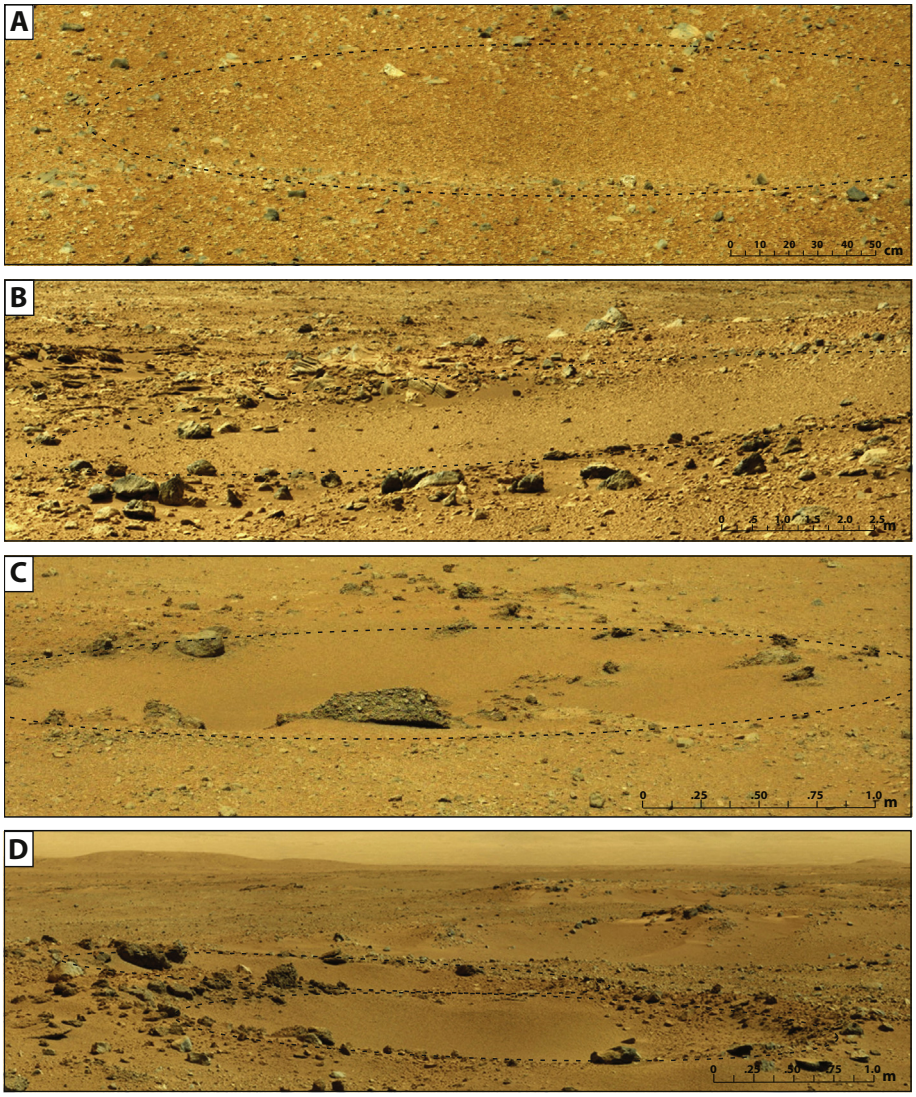


**Fig. 8.** Craters outlined with dashed lines near MSL's path (see Fig. 8 for location). (A) Crater 1 diameter is 3.4 m. Mastcam images 0021MR0000260100100527E01 and 0021MR0000260110100528E01, Sol 21, portion of mcam00026. (B) Crater 2 diameter is 20 m. Image looking East. Mastcam image portion of M100 mosaic mcam00248, Sol 54. (C) Crater 3 diameter is 16 m, portion of 0351ML0014280000108355E01, mcam01428 Sol 351. (D) Image of two craters, crater 4 in the foreground is 4.7 m in diameter and Crater 5 in the background is 4.7 m in diameter. Portion of 0364ML0014810320108590E01 and 0364ML0014810330108591E01, Sol 364. Images: NASA/JPL-Caltech/MSSS.

or vertical surface to cause abrasion and produce ventifacts is discussed in Laity and Bridges (2013) and is akin to sandblasting. The effect depends on the presence of sand, as areas with only dust do not have ventifacts. Saltating sand has a prominent kinetic energy that peaks at a maximum a few 10s of centimeters above the surface, from the combination of particle concentration and the kinetic energy of individual particles. The current form of the most degraded craters is therefore due to enhanced removal of the crater rims and infilling of the depression (e.g., Fig. 9A). Some degraded craters appear to retain remnants of layered infilling deposits of uncertain origin (Williams et al., 2013), which are currently undergoing aeolian excavation accompanied by trapping of windblown sediment in protected lows. The presence of bright dust in some deeper craters along the traverse suggests the process mobilizing the regolith is currently inactive. Large clasts on the floors of some craters, such as the prominent light toned blocks in and on the rim of Craters 4 and 5 could reflect addition of materials from proximal or distal ejecta (Fig. 9D). Wind can also modify the shape of small craters, with the downwind rim experiencing preferential erosion (Kuzmin et al., 2001), but this effect is not observed to be prevalent at the location of the Curiosity traverse.

A major effect of the small impacts observed during the first 360 Sols is the excavation and displacement of large blocks of bedrock, commonly exposed on rims of the craters as described above. These materials are bedrock clasts that have been fractured and faulted on local scales which can be termed autochthonous impactites (Grieve and Therriault, 2013). In terrestrial craters the degree of brittle deformation increases as the crater rim is approached (Grieve and Therriault, 2013). In addition to the blocks associated with craters, numerous blocks of bedrock materials were observed whose tabular aspect ratios and tilted bedding surfaces estimated from stereo images are possibly consistent with an origin by impact, even though they are not associated with an extant crater. Examples of the isolated tilted blocks of conglomerates include the Little Bird sample (Fig. 9D), and the rocks named Link (Fig. 9E), and Hottah (Fig. 9F) (Williams et al., 2013). The similarity of these blocks to the local bedrock suggests a local origin, as opposed to other blocks of apparent igneous origin discussed below. These examples all show non-horizontal dips, in contrast to the generally horizontal dips of beds at the landing site and in the Glenelg and Gillespie deposits closer to Yellowknife Bay. Because in-place bedding adjacent to the blocks is not visible for these examples, a

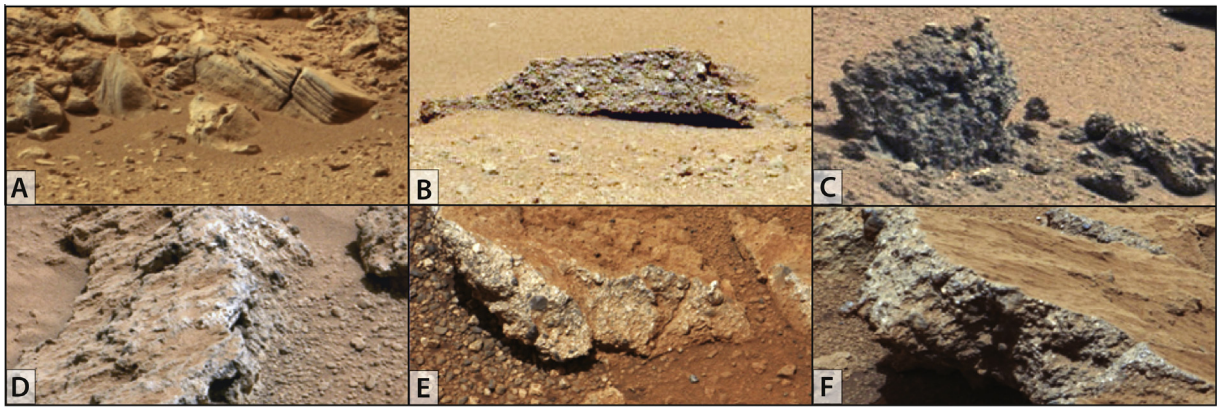


**Fig. 9.** Bedrock materials possibly associated with cratering processes. (A) Image of upturned layered bedrock to angles 40–80° (Shaler facies) associated with a 20 m diameter crater shown in Fig. 8B. Portion of Mastcam 0054MR0002480090103042E01, Sol 54. Image 1.8 m wide. (B) Conglomerate blocks on the rim of a 16 m crater rim tilted ~20° away from the rover (Fig. 8C), portion of 0349ML0014210040108345E01, Sol 349. (C) Upturned conglomerate blocks along rim of a 4.7 m diameter crater. The large original orientation of the large block cannot be determined, but the smaller flat block to the right is tilted 30°. Image width 1 m. (Fig. 8D), portion of 0365MR0014820070301453E01, Sol 363. Image width 0.6 m. (D) Little Bird River outcrop showing a slab of conglomerate dipping ~20° that is not associated with a visible crater. Image portion of 0358MR0014590010301306E01, Sol 358. (E) Conglomerate block dipping >50°, termed Link, not associated with a visible crater, portion of 0027MR0001290050100755E01, Sol 27. Image width 0.2 m. (F) Conglomerate outcrop block, called Hottah, dipping ~20°, not associated with a visible crater, portion of 0039MR0001770070101226E01, Sol 39. Image width 0.2 m. Images: NASA/JPL-Caltech/MSSS.


**Fig. 10.** Bedrock blocks showing an offset that could be due to impact effects. Mastcam image 0053ML0002440190102239E01, Sol 53, scale bar 0.2 m. Image: NASA/JPL-Caltech/MSSS.

depositional origin for the tilt of the beds is also possible. Alternative origins by erosional displacement or faulting also cannot be ruled out, but the examples described are not located near scarps or obvious linear fracture zones.

Another type of bedrock disruption (or fracturing), probably due to impacts is represented by the set of offset blocks of fine-grain sandstone observed on Sol 53 (Fig. 10). Alternative explanations in addition to erosional displacement for this disruption could include mass movements associated with basement related faults or large scale mass movements originating in Mt. Sharp or the crater rim, but these explanations seem very unlikely for this particular outcrop given the embedded nature of the outcrop. The potential role of ice and periglacial effects cannot be ruled out (Fairén et al., 2014), but these processes are probably more relevant to the origin of some types of surficial breccias with angular clasts (see below). At present, no evidence of mass wasting events has been proposed for this portion of Gale, but such events might have been possible earlier, especially before the lower flanks of Mt. Sharp became more eroded.

A search for very small craters less than 2 m in diameter was conducted, but the irregular surface of the HP unit in particular makes identification of these craters from the vantage point of the rover difficult unless they are in close proximity. The smallest crater identified in the rover images, at 0.6 m diameter, and less than 0.1 m deep is illustrated in Fig. 11. Another example of a small crater 1.2 m diameter and ~0.2 m deep, close to the Rover was seen on Sol 494 in NavCam images (NLB_441350284RASLF0250000NCAM00250M1). The size of craters on the surface, particularly at the smaller diameters, is

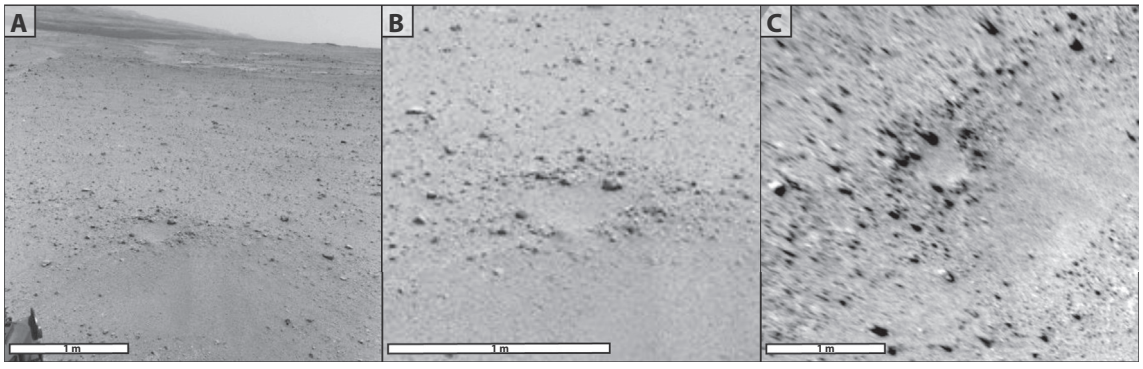


**Fig. 11.** A 0.6 m diameter crater on the rim of a larger crater. (A) Navcam frame from Sol 338, NLB_427502017RAS_F0080610NCAM05114M1. (B) Enlargement of the small crater from the same frame. (C) Vertical projection with north up, showing the circular expression of this small crater. Images: NASA/JPL-Caltech.

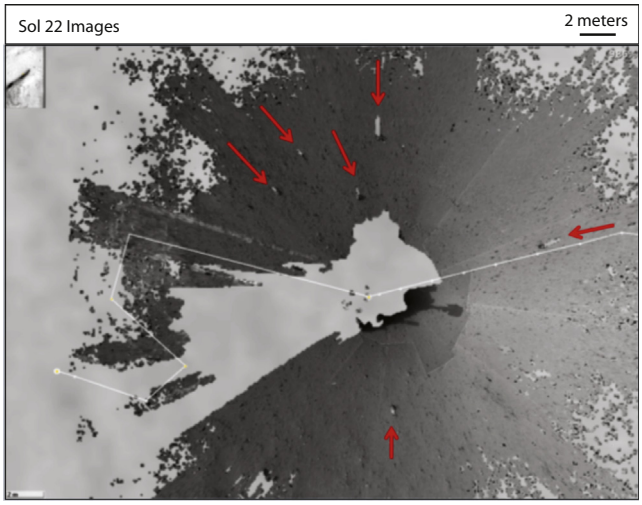


**Fig. 12.** Example of a map projected Navcam mosaic image from Sol 22. The locations of six rocks larger than 20 cm are indicated by arrows. The radial light "shadow" extending from the rock locations represents the projected map area hidden by the rocks.

modulated by the atmosphere, and theoretical calculations suggest there should be a cutoff at a diameter of ~20 cm (0.2 m) (Vasavada et al., 1993; Williams et al., 2012). However, extensive surveys of the MER images (Paige et al., 2007) do not reveal candidate hypervelocity craters at centimeter scales. Our more limited observations of an area ~3800 $m^2$ (roughly the area of a football or soccer field) do not reveal relatively fresh candidate craters smaller than ~0.6 m in Gale crater (Fig. 12), so our more limited data set is consistent with the MER results. Oblique craters less than ~1 m in diameter are unlikely to occur, because atmospheric slowing of a small oblique impactor will dramatically reduce the velocity and energy of the particle and also lead to a vertical impact. On the lunar Maria continuous exposure to impacts has resulted in an impact-generated regolith that can be several meters thick (McKay et al., 1991). The absence of a thick regolith seen by Curiosity is related to the absence of small craters and is therefore consistent with the long term presence of an atmosphere, and perhaps also to the ongoing aeolian exhumation of the surface under investigation by Curiosity.

## 6. Crater degradation and resurfacing rates at Gale crater

At Gale, the history of the most recent alluvial materials starts with the counts on Aeolis Palus (the floor or moat of Gale) of craters >400 m in diameter, which gives an age of 3.2–3.3 Ga (Grant et al., 2014). Impact craters have a depth of ~0.2 times their diameter (Kenkmann et al., 2013), and the counts of large craters suggest that a maximum of 20–40 m of erosion or burial occurred since 3.2–3.3 Ga, otherwise the number of large craters would be lower. Another detail from the investigation of larger craters by Grant et al. (2014) of the upper Peace Vallis fan (not visited by Curiosity), is the evidence for late burial by an additional 10–20 m of presumably alluvial materials, with a subsequent 5 m of erosion. In contrast the BF unit visited by Curiosity in the Yellowknife Bay area does not show evidence of a late burial. The low slope of the crater size–frequency distribution (Grant et al., 2014) suggests more continuous erosion since deposition with the same constraint of a maximum of 20–40 m of erosion since 3.2–3.3 Ga. The crater counts are consistent with the geological evidence of Palucis et al. (2014) for on-going exhumation of the BF unit.

The mechanisms of resurfacing may be somewhat different for the two different areas visited by Curiosity. Unfortunately, no craters were examined by Curiosity in the BF unit up close, and the cumulative area observed within 25 m of the rover was limited. In contrast to the HP unit, strata of the BF unit appear to lack the availability of erosionally resistant bedrock blocks that commonly form a resistant lag or ring of blocks on the crater rims as seen on the HP unit (Fig. 9). Therefore, on the BF mudstones, the loose sediment making up the crater rims of small (<10–15 m diameter) craters is easily removed by aeolian erosion, greatly reducing the visual evidence for the craters compared to similar craters on the HP.

On the Hummocky Plains unit, near and to the west of Bradbury Landing (Calef et al., 2013; Sumner et al., 2013), blocks of conglomerates and sandstone of likely alluvial origin are present (Williams et al., 2013). Large blocks are especially abundant around craters, although processes that could result in the presence of loose blocks on the surface include fault displacement, including movement along listric and normal faults formed as part of the crater terrace formation, landslides (observed on the slopes of Mt. Sharp, but not adjacent to the area of the Mars Science Laboratory), and undermining of resistant ledges by erosion (many examples along the traverse). In the absence of observable faults, lobes of landslide or debris flow material and nearby erosional scarps, impact processes are the most likely sources for the observed blocks. Impacts into the resistant sandstone and conglomerate bedrock on the HP results in the common presence of rocky rings on the rims that are harder to erase than craters of the BF in Yellowknife Bay, at least when viewed from the rover perspective.

Under the influence of erosional processes, the predominant conglomerates and sandstones of the HP unit behave differently from the mudstones and sandstones of the BF unit visited in Yellowknife Bay. On the Hummocky Plains, removal of craters by rim erosion and infill is suggested by the observations from the Curiosity rover described above (Figs. 8 and 9). The removal by abrasion of the blocks found on crater rims is governed by the aeolian processes discussed at length by Bridges et al. (2014), which leads initially to the formation of ventifacts. Therefore, on the HP unit, the resurfacing rate consists of multiple processes, including enhanced aeolian erosion of crater rim material and projecting blocks, erosion on the floors of valleys that concentrate mobile sand deposits, and aeolian deposition in craters and swales. Additional variations in degradation are related to topography and prevailing wind directions that may affect the location of enhanced erosion on crater rims, ledges, and deposition of material within craters, valleys and depressions. The effects of later impacts can include destruction of earlier craters, and deposition of ejecta on top of earlier craters, but the low abundance and spatial distribution of craters less than 10–15 m diameter, suggests this process is of negligible importance in this setting. Even in cases where small impacts not identifiable from orbit have occurred on the HP, their identification from the rover can be difficult beyond 5–10 m from the rover, although the irregular surface may retain evidence of their disruptive effects (e.g. Fig. 9D).

Combined observations from orbit and from Curiosity constrain the resurfacing rates at Gale crater. These rates should be faster than the rates observed on the Moon, where resurfacing rates due to impact cratering range from 0.2 to 0.5 mm/Myr (Craddock and Howard, 2000; Fassett, 2013). Even assuming an increase on Mars by approximately a factor of 2.6, due to the proximity of the asteroid belt, impact resurfacing rates alone would only be 0.5–1.3 mm $Myr^{-1}$, and this rate is still probably too large because it includes the effects of the smallest projectiles which are filtered by the martian atmosphere (Soderblom, 1970). This rate is clearly a lower limit for Mars, as the resurfacing rate is dominated by aeolian deposition and erosion.

The dominance of aeolian erosional processes is consistent with the geomorphology of the areas imaged by the rover and studies

elsewhere on Mars, including the presence of abundant ventifacts (Bridges et al., 2012; 2014; Bridges and Laity, 2013). An analysis of the topography of the Peace Vallis Fan (Palucis et al., 2014), suggests substantial deflation, based on the presence of inverted channels, and erosional scarps. This analysis shows that 80% of the lower Peace Vallis fan, containing the BF unit, is eroded by less than 5 m. Although there are areas in the lower fan deflated by more than 5 m, most of the area used for crater counts by Grant et al. (2014) represent areas with less than 5 m of erosion. The BF unit exhibits slightly lower crater abundances for craters >15 m diameter than the HP unit (Fig. 4), suggesting that this unit has had less time to accumulate small craters due to more recent exhumation, and/or the possibility that craters may be more easily erased by erosion in the BF unit (Palucis et al., 2014). Based on an age of 3.2–3.3 Ga for the sediments, and an estimated maximum burial depth of 20–40 m for the surface of Yellowknife Bay (including the missing 5 m), an average erosion rate on the order of ~8–14 mm/Myr is required to get down to the current surface. This erosion rate from Gale is consistent with the range of rates (1–30 mm/Myr), estimated by Golombek et al. (2006a,b, 2014) including rates from the last 100 Myr, and the rates averaged over the last 3 Ga, derived from multiple sources and landing sites and is representative of the Hesperian and Amazonian on Mars.

Constraints on more recent erosion rates can come from the 78 Myr cosmogenic nuclide exposure age results from Farley et al. (2013) on a sample derived from the Cumberland Drill site. Cosmic-ray-produced $^{3}$He, $^{21}$Ne, and $^{36}$Ar yield concordant surface exposure ages of 78 ± 30 Ma. Based on this data, the mudstone is considered to have been rapidly exhumed from approximately 2–3 m depth to the surface ~78 Myr ago. Farley et al. (2013), ascribes this to retreat of a scarp that is now about 60 m from the drill site. Converting this age to a vertical erosion rate, assuming a scarp retreat model, involves an assumption about the fraction of exposed bedrock older and younger than 78 Myr. Assuming that the young surface area exposed in the last 78 Myr is 10% of the total area of the lower Peace Vallis fan, then the average exposure age of the upper 2–3 m of the surface is 390 Myr. (Note that the crater retention age of the sediments can be much older.) Therefore, assuming 2.5 m of erosion in that time period a rate of 6 mm/Myr is obtained. This result is reasonable from a geological point of view given the proximity of the Cumberland sampling site to the scarps around the edge of Yellowknife Bay. This value is highly uncertain (factor of 10) given the uncertainty on the age, the unknown actual depth of erosion, and the unknown fraction of the area older than 78 Myr. However, the rate is plausibly similar to the maximum average rate of 8–14 mm/Myr determined above for erosion of ~40 m of sediment since 3.2 Ga.

## 7. Comparison to Mars Exploration Rover mission craters

The MER missions examined numerous small impact craters (Grant et al., 2006a; Golombek et al., 2006a,b) with results relevant to craters observed by Curiosity, including the recognition of the substantial control of crater excavation by the fractures in the basement that penetrate the bedrock (Watters et al., 2011). In the case of the 150 m diameter Endurance Crater on Meridiani Planum, the presence of orthogonally oriented basement fractures led to highly asymmetric excavation, with limited subsequent modification by erosion (Watters et al., 2011). Structural control of the craters observed in the area near the Curiosity traverse (e.g. Fig. 7) cannot be confirmed although these craters are also commonly irregular in shape. However, the craters examined during the rover traverse are smaller than Endurance, and the effects of aeolian erosion and deposition have had a greater effect on the shape of their rims, ejecta blankets, and fill.

As summarized from Grant et al. (2006a) impacts into the basaltic plains of Gusev crater create shallow craters and ejecta comprised of resistant rocks, such as the rock Mazatzal (Squyres et al., 2004). Initial aeolian stripping of ejecta quickly becomes weathering-limited as lags develop and most available sediments become redistributed and trapped within craters. Due to the flat topography, aeolian modification is accompanied by only minor mass wasting, and there is no evidence for modification of crater forms by water. By contrast, the variable slopes, target lithologies and availability of mobile surficial deposits in the Columbia Hills within Gusev crater lead to less uniform degradation rates from crater to crater and within craters.

At Meridiani, relatively low strength rocks forming crater rims, exposed walls, and ejecta are more rapidly stripped by the wind, while lower, more protected crater interiors are increasingly infilled and buried by mostly basaltic sediments and more resistant fragments (e.g., hematite spherules) (Grant et al., 2006b). Aeolian processes outpace any early mass wasting of crater walls, which typically leads to meters of erosion (locally) and wholesale mantling that likely account for complete removal/burial of some craters. As at Gusev, many larger craters in Meridiani experienced greater net degradation than smaller craters, but still display a less degraded form due to the larger scale of the primary impact features.

Overall, the range in degraded crater forms within Gale exceeds that of either Gusev crater or Meridiani Planum. Such variation is not unexpected given the broader range in impact lithologies, local topographic setting, and history of geomorphic activity that may have included alluvial infilling. Hence, it can be more difficult to identify the form of individual craters within a degradational spectrum related to age. As noted above, craters formed in less resistant materials, such as were encountered in Yellowknife Bay, or Meridiani, may be wholly removed by erosion over a geologically short period of time, whereas craters formed in more resistant and/or well-cemented targets can retain relatively pristine morphologies over substantially longer geologic periods.

## 8. Isolated blocks on the Hummocky Terrain

During the rover traverse across the Hummocky Plains, isolated blocks (>20 cm in length) that appear to be float not connected to the local bedrock were observed. These rocks often have sloping faces indicative of wind erosion, but are clearly more resistant than the underlying materials. Many of these samples, at ranges of less than 6 m from the front or sides of the rover were analyzed and imaged by the ChemCam instrument as described below. To better understand the areal abundance of these blocks, a survey was conducted of the abundance of blocks (>20 cm in length) visible in the regular and vertically projected NavCam mosaics (e.g. Fig. 12) around the stops on the Hummocky Plains up to Sol 361 (Table 1). Stereo NavCam images are a significant advantage in identifying surficial blocks relative to single black and white NavCam images, in which the blocks can often have the same brightness, contrast, and texture as surrounding materials. The survey included blocks to a maximum distance of about 18 m from the rover (see Section 2 for sources of images and methods). The surprising result of this analysis was the relatively low abundance of these blocks, except in the area of the slope down to Yellowknife Bay. Some increases in the number of large nearby blocks occurred in the vicinity of the ridges informally named Twin Cairns Hill, Elsie Mountain, and Mealy Mountains, but only in one of these cases did the immediate vicinity of the Rover contain as many as 16 large blocks. On average, only ~2.5 blocks per 100 m$^2$, were present in the vicinity of the rover at 24 locations. Excluding Sol 340, the number is ~2 blocks per 100 m$^2$. An area of 100 m$^2$ is roughly the area in the ChemCam targetable area around the rover.

Most large blocks along the traverse (>20 cm) were avoided for rover trafficability. Thus, most of the blocks analyzed from a close distance by Mastcam and ChemCam during the traverse are actually smaller than 20 cm. While these small rocks may include samples of local derivation, many rocks display a dark surface, rough texture, and wind borne dust abraded faces such as Jake_M, Coronation, and Mara (Fig. 13A–C) (Bridges et al., 2014). Wind abraded surfaces can reveal the texture of the rock interior in many cases. The surfaces of the isolated blocks appear to include either sedimentary or igneous textures.

Identification of sedimentary textures includes the presence of layering and a fine-grain texture consistent with bedrock outcrops of sandstones observed at close range (e.g. Mangold et al., 2014; Anderson et al., 2015), or a conglomeratic texture (e.g. Williams et al., 2013). Conglomeratic outcrops have variable clast sizes, shapes, and colors. The most definitive conglomerates observed early in the mission are characterized by abundant pebbles 2–40 mm diameter, classified as subrounded or rounded (Williams et al., 2013). Kasegalik (Fig. 13I top) is a layered rock observed on Bradbury Rise lying next to the conglomerate boulder, Kaniapiskau (Fig. 13I bottom). Bedrock outcrops of similar lithologies occur along the rover traverse. ChemCam data show that Kasegalik has the same composition as the top-most section of the Yellowknife Bay sediments, namely Bathurst, and other float

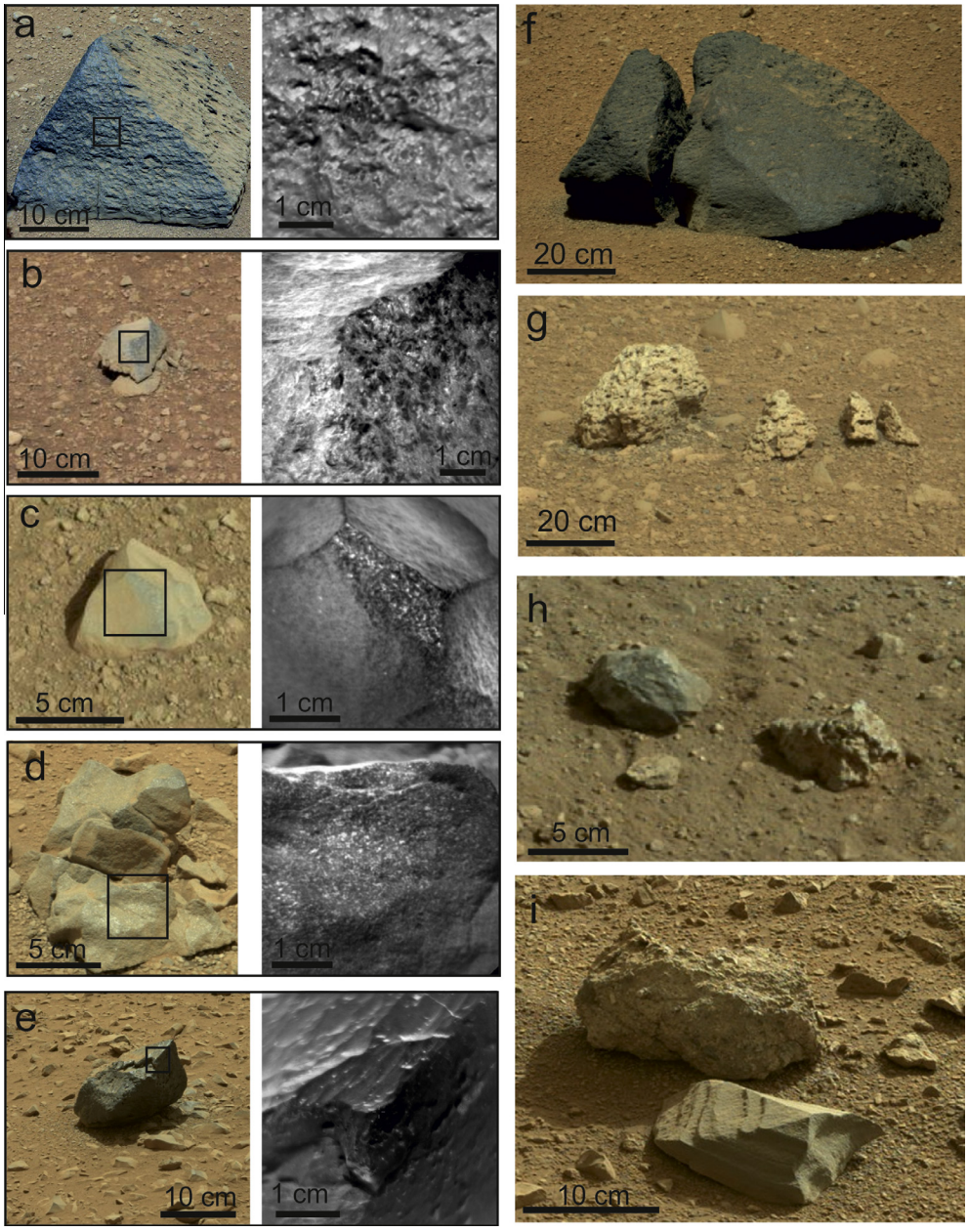


**Fig. 13.** Float rocks observed on the surface by Curiosity. From (A–E), combination of Mastcam (left) and ChemCam/RMI close-ups on a series of float rocks. (F–I) Portions of Mastcam images of float rocks. Sol indicates the martian day (A) Jake Matijevic, portion of Mastcam 0044ML0002040000102078E01, Sol 44. (B) Mara, portion of Mastcam 0003ML0000000760100096E01, Sol 3. (C) Coronation, portion of Mastcam 0003ML0000001140100134E01, Sol 3. (D) La Reine, portion of 0346ML0014050000108270E01, Sol 346. (E) Watterson portion of Mastcam 0327ML0013290030107883E01, Sol 327. (F) Bull Arm, portion of 0349MR0014160000301161E01, Sol 349. (G) Unnamed rocks, portion of 0020ML0000570050100410C00, Sol 20. (H) Unnamed rock (left) and Stark (right), portion of 0003ML0000000950100115E01, Sol 3. (I) Kasegalik (bottom, layered sediment) and Kaniaspakau (top, conglomerate), portion of Mastcam 0335MR0013510000301054E01, Sol 335. Images: NASA/JPL-Caltech/MSSS, NASA/JPL-Caltech/LANL/CNES/IRAP/IAS/LPGN/CNRS/LGLyon/Planet-Terre.

similar in texture found close to Bathurst (Mangold et al., 2014). How the blocks came to be in close proximity is unknown, but local impact processes are a likely explanation.

Igneous textures were displayed by numerous blocks examined by ChemCam on Bradbury Rise (Fig. 13A–E). The adjacent unnamed rocks (Fig. 13G) observed along the traverse on Sol 20 are sitting on a low rise, less than half the height of the blocks (based on stereo imagery); the rise is possibly protected from erosion by the presence of the blocks. The pieces are clearly from one original rock, based on the texture, and the original block may have been broken in four pieces by ballistic impact, or simply been eroded into the remnant blocks. Some of the blocks (Fig. 13F and G) display vesicles or voids suggesting gas escape or dissolution. The difficulty of determining the origin of the holes makes it premature to infer a relationship to the tops of a lava flow. Although the rocks in Fig. 13G were not analyzed by ChemCam, the light-toned rock on Fig. 13H (to the right), named Stark, shows surprisingly high silicon content indicating a felsic composition. ChemCam analyses of igneous materials on the Hummocky Plains seem to generally reflect a felsic composition (Williams et al., 2013; Meslin et al., 2013; Sautter et al., 2014).

The first rock examined in detail by Curiosity, named Jake Matijevic (Jake_M), has an igneous texture on the surface observed at MAHLI scale, and an alkali-rich composition deduced from APXS and ChemCam chemistry (Stolper et al., 2013). The rock Mara (Fig. 13B) exhibits a coarse-grained texture typical of slowly-cooled magmatic rocks, including dark millimeter-wide phenocrysts typical of mafic phases (i.e., pyroxene or olivine), separated by light-toned matrix likely dominated by feldspars (Sautter et al., 2014). Coronation and La Reine (Fig. 13C and D) display similar dark/light grain assemblage but with smaller grains (200–500 μm) still visible at RMI scale. Such texture is typical of high-level intrusive (hypabyssal) magmatic rocks, such as diabase. Despite these two rocks being separated by 300 m of terrain, their similarity suggests a common source. In addition to a strictly igneous origin, there is also the possibility that some of the rocks could represent impact melts with porphyritic textures, glassy fine-grained melts, and/or basement subjected to impact with accompanying pseudotachylyte veins (e.g., Spray, 2010). Finer igneous-like textures are also observed in many other examples observed by the ChemCam RMI (Sautter et al., 2014). Watterson (Fig. 13E) displays a total lack of grains visible at RMI scale, and displays sharp edges and conchoidal fracturing, suggesting a predominance of glass, such as for rocks derived from quickly-cooled lava flows or impact melts. The lack of flutes argues against an abrasion origin for the texture. Bull Arm (Fig. 13F) is one of the larger dark rocks to be observed, showing strong similarity in composition to Jake_M. Its division into two pieces may reflect either fracturing during ballistic impact, or thermal cracking (c.f., Eppes et al., 2010).

An origin for the larger surface blocks (>20 cm) as proximal ejecta from a nearby km – size crater can be ruled out due to the lack of large local craters and low block abundance compared to terrestrial analogs such as Lonar Crater, India (Newsom et al., 2013a,b), or Gusev crater. At Gusev, Grant et al. (2006a) measured the abundance of blocks >15 cm on the Gusev Plains and Husband Hill from MER Spirit observations, and the abundance was much greater than measured at Gale, ranging between 20 per 100 $m^2$ on crater ejecta to 30–35 on the volcanic plains and on Husband Hill, to just over 50 for counts along crater rims. The larger blocks with igneous textures on the surface of the Hummocky Plains may therefore represent a lag of distal ejecta from large craters, or a remnant of a discontinuous ejecta deposit from impact craters outside of Gale crater. Many of these blocks appear to be crystalline igneous rocks, like Jake_M, and are consistent with an origin as distal ejecta blocks, as none of the in-place bedrock observed so far is conclusively determined to be igneous in nature. Additionally, these larger blocks are distributed relatively uniformly across the surface of Bradbury Rise, in contrast to clasts interpreted to be sedimentary in origin, which are more closely associated with bedrock outcrops from which they might derive (Yingst et al., 2013).

If the isolated blocks identified above represent ballistically-transported blocks, they could provide information regarding the regional geology. Gale is located at the edge of the dichotomy boundary, mainly in the Noachian highlands. It is, therefore, surrounded by Noachian crustal terrains to the south, west, and east, and younger volcanic plains to the north (Fig. 1). The closest sizable crater is 4 km in diameter, and is located 15 km to the west of the landing site on the floor of the crater and may have provided ballistically derived material that could potentially contain materials from the floor of the impact crater, including impact melts and reworked ancient crust (e.g. Schwenzer et al., 2012). Further from the landing site, but within 3.5 crater diameters to the north east, is a prominent 23 km diameter crater that may have provided ejected material to Gale. This breadth of potential source material is likely reflected in the textural and chemical diversity of materials encountered by Curiosity. For example, the coarse-grained and porphyritic textured rocks could be ancient Noachian crust and the finer grained material could be volcanically derived material given the proximity of the Elysium volcanic province a few hundred kilometers to the north of the crater. The next closest large volcanic province is Tyrrhena Patera, but this is 2000 km away.

One class of dark blocks (e.g. Fig. 14) of uncertain origin was observed primarily at the top of the low ridges making up Twin Cairns Hill, Elsie Mountain, Mealy Mountains, and Mt. Kennedy.

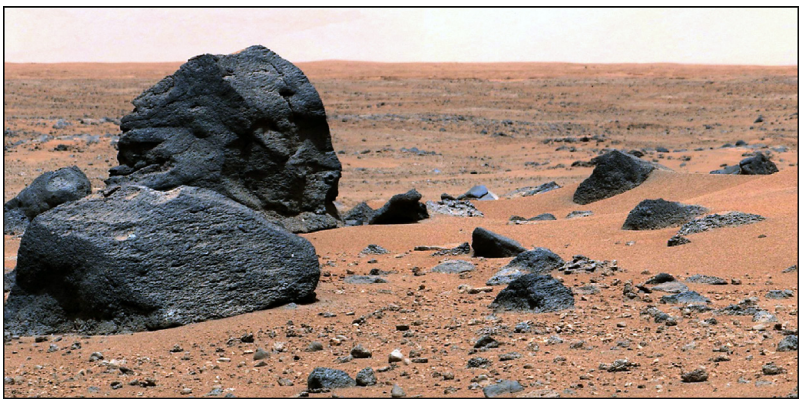

**Fig. 14.** Portion of MastCam M100 mosaic (mcam01420) of an outcrop named Elsie Mountain, taken on Sol 349. The rocks range in size from tens of centimeters to approximately one meter in width and are vuggy with coarse layering.

These ridges and mounds were observed beginning at Sol 345, and extending beyond Sol 360. The ridges probably represent inverted topography with capping blocks that are resistant to erosion. The maximum size of the measured blocks on all of the ridges is approximately one meter in most cases. The possible origin of these rocks includes sediments, impact ejecta debris, or volcanic material. However, analysis of similar rocks by ChemCam (Sautter et al., 2014) indicates compositions related to Jake_M, which could be consistent with an igneous protolith, although a sedimentary origin cannot be ruled out. The very similar maximum size of these blocks and their apparent location at one stratigraphic horizon argues against an impact origin. Further investigation of isolated blocks by Curiosity and comparison with the chemical and spectroscopic properties of the nearby crust will be needed to determine what classes of blocks are consistent with a local origin within Gale, or a distal origin.

## 9. Possible impactite materials observed by Curiosity

Impactite materials seem to be surprisingly uncommon in the areas studied by Curiosity given the size of Gale crater and the large number of superimposed craters. Impactite materials include shocked minerals, impact melt, impact melt bearing breccias, shatter textured rocks and shatter cones. For this study, every Mastcam and RMI image of terrain within about 25 m of the rover during the first 364 Sols has been examined for impact materials. In general, the NavCam images are too low in resolution for identification of impact-related materials. Even the Mastcam images are also often too low in resolution due to distance of the targets, image compression, and there are operational and strategic constraints that usually prevent use of a bump to approach all but the highest priority targets, such as drill sites. Because the coverage of the MastCam (and RMI) is very limited close to the rover, the area surveyed is much less than the area examined for the large block survey which utilized the 360° NavCam mosaics. Due to these limitations, it is not surprising that the survey turned up very few candidates, but the examples are illustrative of what can be seen with the available data.

Possible examples of shatter cones and shatter-textured rocks are seen in Fig. 15A and B. Conical striations in the sample in Fig. 15A are reminiscent of shatter cones. Shatter cones are best developed in fine-grained sedimentary rocks in terrestrial craters, but are also found in fine-grained igneous or metamorphic basement rocks commonly exposed in central uplifts (Ferrière and Osinski, 2013). Shatter cones are distinguished by divergent striations that appear to penetrate the rock, in comparison with slickensides with parallel striations, or ventifacts, where surficial textures are caused by aeolian erosion (Ferrière and Osinski, 2013). Although well-developed shatter cones are very distinctive visually, less developed shatter cones and shatter textured rocks (rocks with subparallel lineations) are common at terrestrial craters but are mainly recognized due to their proximity to other evidence of impact. Stereo imaging of candidate shatter cones by the RMI or MAHLI cameras should be able to resolve the diagnostic features, but candidate samples have not yet been examined in this way. Fig. 15B shows an example of a rock with striations that could be related to shock, but the image resolution is not sufficient to confirm the nature of the striations, in particular to distinguish them from aeolian abrasion features. The limited number of candidates is not surprising, because shatter cones are usually associated with bedrock from beneath the transient cavity of relatively large craters, including the central uplift (Ferrière and Osinski, 2013). Such materials would not be expected in the locations visited by Curiosity unless transported from the crater rim as distal ejecta. Fluvial transport would expose the samples to substantial erosion destroying the subtle textures.

Rocks that have been shocked, but not actually melted, represent another class of impact-related materials. Martian meteorites are commonly shocked to high pressures (~30 GPa), at which point compressible minerals like feldspar begin solid-state transformation to an amorphous state, leading to the formation of the pseudomineral maskelynite, which was originally observed in the Shergotty martian meteorites (Tschermak, 1872; Stolper and McSween, 1979). The surface expression of shocked rocks can include penetrative lineations called shatter texture, possibly represented by the sample shown in Fig. 15C. Basement rocks that have been shocked commonly contain veins of impact melt or hydrothermal alteration phases which potentially result from impact hydrothermal processes or impact melt injection of bedrock lithologies. A possible example is seen in Fig. 15E. However, the light toned lathes in the sample are more likely feldspar grains, being similar in grain size (1–2 mm wide by up to 10 mm in length), as those seen in much more detail in the rock Harrison observed on Sol 514 later in the mission (http://solarsystem.nasa.gov/multimedia/display.cfm?Category=Planets&IM_ID=18767). Shocked rocks can also exhibit vesicular textures if they reach a state of partial melting. Such shocked rocks often weather heterogeneously, as suggested by the Little Wind River sample (Fig. 15E). Only fragments from one candidate Fe-rich meteorite have been identified in images from Curiosity to date (Sol 637, images 0637MR0027090010401814E01 and 0637MR0027090040401817E01), although several meteorites have been identified by the MER rovers (Schröder et al., 2008).

Crystalline rocks shocked to even higher pressures (50–60 GPa) can produce impact melts. Impact melts from crystallized coherent sheets can often look like porphyritic igneous rocks (Therriault et al., 2002; Spray et al., 2010), making image identification difficult. Distinguishing such materials from igneous rocks is probably not possible with the payload of Curiosity. Impact melts that have not recrystallized often contain ropy-textured materials similar to lava flows or pyroclasts (cf. Newsom et al., 2013a,b). Candidate examples are shown in Fig. 15F–H.

Impact melt-bearing breccias are likely to be present in the ejecta blankets of craters on Mars, but their identification requires confirmation of the presence of glass (and possibly nickel from an impactor). Impact melt-bearing breccias are often called "suevite", after their occurrence at the Ries impact structure in Germany. However, as discussed by Grieve and Therriault (2013): "The current literature record and the use of the term 'suevite' are inconsistent and somewhat confusing. Until there is a better understanding, it may be best that the term suevite be reserved for the original occurrences at the Ries. Other occurrences should be referred to more generically as melt – bearing breccias."

Many examples of clastic breccia have been observed, beginning with the Goulburn deposits exposed at the landing site. The presence of rounded clasts in most of these deposits suggests that they are actually conglomerates of fluvial origin such as Link and Hottah (Williams et al., 2013). However, there are examples of other breccias (e.g., Fig. 15I and J), containing a combination of large, angular clasts and a wide range in clast sizes, that may provide the best candidates for impact ejecta, although such associations do not uniquely discount hydraulic transport (Whiting et al., 1988). On the lunar Maria, continuous exposure to impacts has resulted in an impact-generated regolith that can be several meters thick (McKay et al., 1991). The absence of a thick regolith in Gale is consistent with the burial and relatively recent exhumation of the bedrock under investigation by Curiosity.

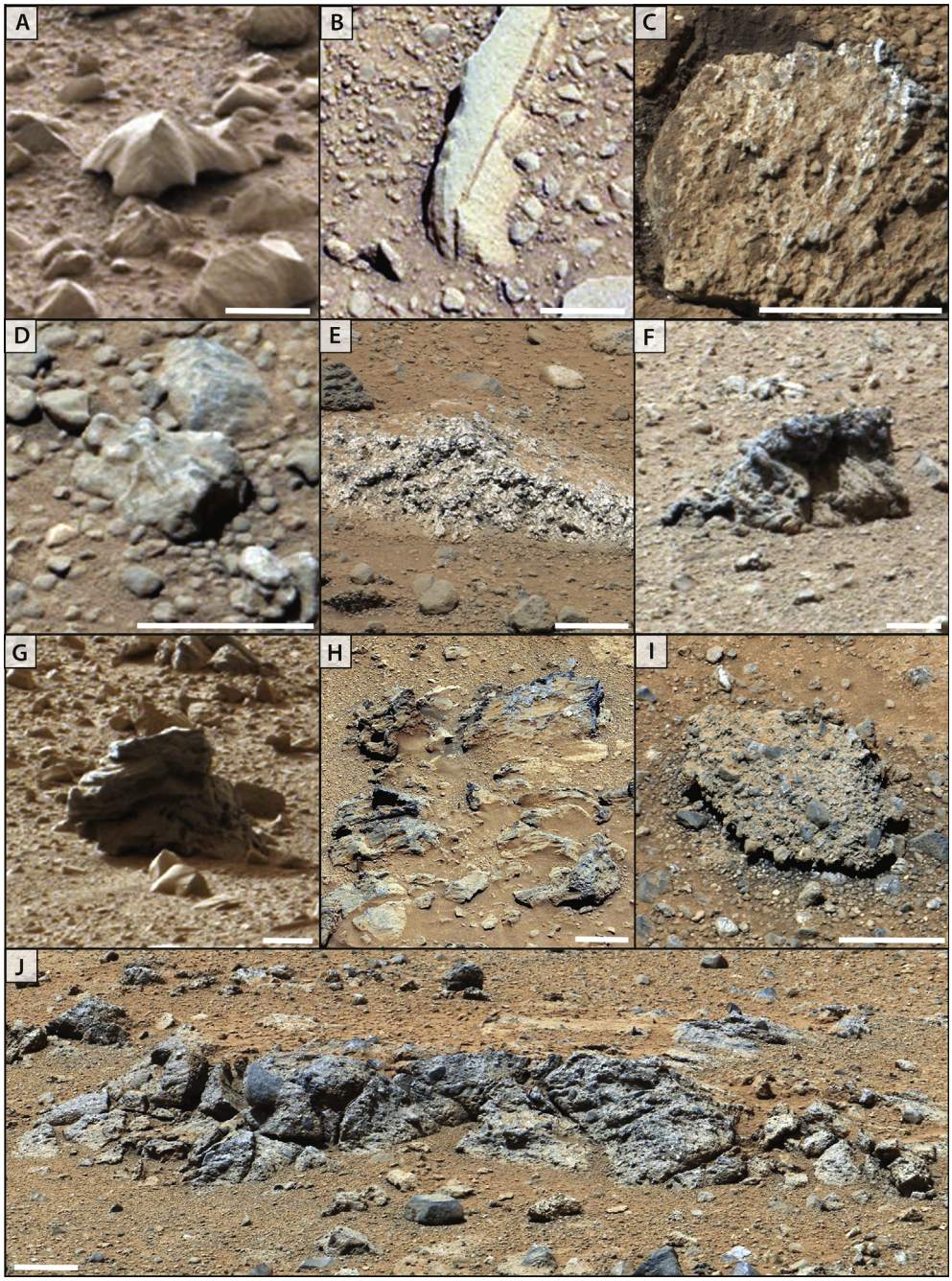


**Fig. 15.** Candidate impact materials observed by the Curiosity rover. (A) Possible shatter cone showing multiply oriented, striated surfaces that appear to penetrate the rocks (e.g., arrows), which are not generally observed in ventifacts, although the samples lack the most distinctive horse-tail textures of well-developed shatter cones, these might be present on the front face of the rock; Mastcam image 0044ML0001990000102057E01, Sol 44; scale bar is 10 cm. (B) Striated rock (location between arrows) possibly indicating shock pressures indicative of poorly developed shatter cones; Mastcam image 0053ML0002440220102242E01, Sol 53; scale bar is 2.5 cm. (C) Block disturbed by the rover wheel that is covered with coarse lineations. This texture could potentially be a type of shatter texture, but is more likely an abraded sedimentary surface; Mastcam 0030MR0001350010100768E01, Sol 30; scale bar is 5 cm. (D) Rock with possible veins (arrows), or more likely feldspathic laths as seen in more detail later in the mission on Sol 566; Mastcam image 0339MR0013760010301082E01, Sol 339; scale bar is 2.5 cm. (E) Strongly shattered exposure rock potentially related to shock fracturing; Mastcam image 0358MR0014580000301305E01, Sol 358; scale bar is 5 cm. (F–H) Ropy textured materials potentially representing basaltic impact melt, or primary lava flows; Mastcam images 0036MR0001480010100832E01, Sol 36; 0050MR0002290580102823E01, Sol 50; and 0359ML0014650000108540E01, Sol 359, respectively; scale bar is 5 cm in all 3 images. (I) Possible impact breccia; alternatively, this breccia could represent a clast of cemented duricrust or a conglomerate; Mastcam image 0358MR0014600000301307E01, Sol 358; scale bar is 5 cm. (J) Possible impact breccia or conglomerate containing a wide variety of clast shapes and sizes. Note partly rounded clast indicated with arrow ~4 cm in diameter; portion of Mastcam mosaic mcam01451 (Sol 356); scale bar is 5 cm.

## 10. Spherules, tektites and lapilli

Impact processes can additionally produce small spherical particles of glass resulting from impact-generated melts. The term 'tektite' generally refers to melt particles found at great distance from their source craters, usually implying ballistic transport out of the atmosphere. Similarly, lapilli, associated with proximal ejecta, consist of concentric layers of ash and glass that often adhere to cores of shocked or partially melted rock fragments or melt spherules.

In terrestrial settings, impact spherules and tektites are commonly diagnosed via their distribution in discrete layers, high sphericity, and their association with other fluidal shapes (Glass, 1990; McCall, 2001). Analysis in thin section shows distinctive internal textures (for example quench textures, internal vesicles, and secondary mineral growth that nucleates at the spherule margin (Simonson et al., 2004); see also Type 1 (microtektite) and Type 2 (microkrystite) spherules [Smit, 1999; Smit et al., 1992]). The chemistry can also be distinctive including low water content, elevated $Fe^{2+}$ in glass, and elevated PGE concentrations (Glass, 2002). Unfortunately most of these characteristics cannot be observed by instruments on Curiosity due to the small size of the spherules. Impact spheroids are the form that can most reliably be identified by their shape and surface texture (Yingst et al., 2013; Minitti et al., 2013). Within Gale crater stratigraphy, no discrete horizons of spherules have yet been identified. Rather, candidate impact spherules occur prominently within disturbed soils, such as those found during investigation of the Rocknest wind drift (Blake et al., 2013; Minitti et al., 2013). Such distribution likely reflects a combination of the relatively patchy outcropping along the surface of Bradbury Rise, a relatively thin stratigraphic succession within Yellowknife Bay (<7 m; Stack et al. (2013a)), and ubiquitous dust coverage (commonly clumped into 60–120 μm aggregates; cf., Sullivan et al. (2008) that obscures the shape and surface texture of sand-sized grains. The candidate impact spherules range in size from ~100 to 900 μm. Thus the smallest ones can be segregated onto ripples and be preserved in sand shadows like Rocknest.

Where disturbed, soils comprise a variety of fine sand- to silt-sized (<150 μm) gray, red, and orange–brown lithic fragments; only the larger size fractions are resolvable in MAHLI images (Minitti et al., 2013). Similarly, coarser sand-sized particles comprise a variety of dark gray to gray-white, well-rounded grains, but distinctly not spherical. Within the coarser size material, candidate impact spherules are most readily identified (Fig. 16) by their sphericity and highly uniform surface smoothness, even when sub-spheroidal. In addition, all candidate spherules retain a distinctly glassy, highly reflective surface with a low surface roughness that leads to the preferential loss of dust coating during disturbance. An alternative origin by dust abrasion for the reflective spherical surfaces seems highly unlikely, for particles embedded in the regolith.

Spherules comprise at least 2% of the coarse-grained fraction of surface veneers, and also occur sporadically as coarse constituents within the fine-grained fraction of aeolian accumulations (Minitti

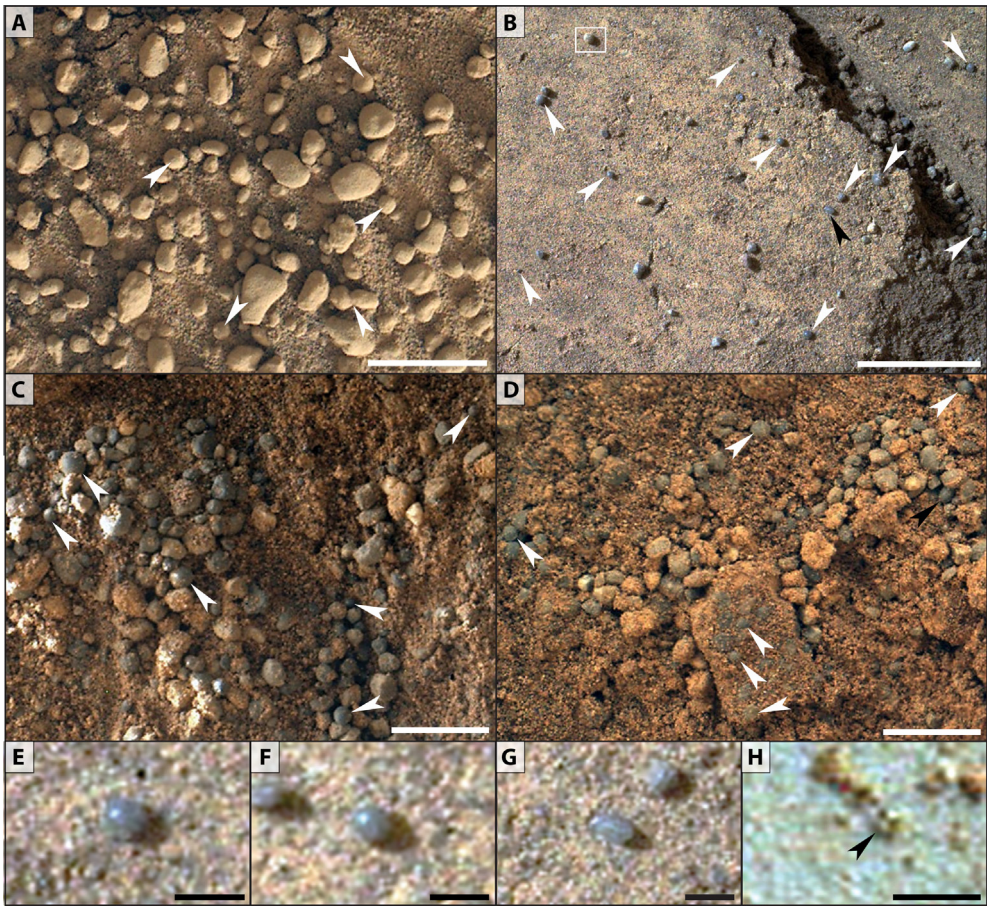


**Fig. 16.** MAHLI images of candidate impact spherules that appear highly spherical and may have a glassy surface. These characteristics, while suggestive, are not proof that every particle identified is of an impact origin. (A) Candidate spherules (arrows) are 1.32–1.65 mm in diameter, consistent with average grain size of coarse-grained sediment that often armors the substrate (Minitti et al., 2013). A coating of dust obscures the characteristic reflectivity of the candidate spherules, although high sphericity can often be inferred from shadowing. Detail of image 0291MH0190001000C0. (B) Abundant candidate spherules from 250 to 700 μm in diameter. (white arrows) atop Curiosity wheel tracks at the Rocknest sand shadow, including ovoid splash forms (black arrow), and a single, highly spherical grain that displays substantially greater surface roughness, such as is observed in armored lapilli (white box). Detail of image 0058MH0032000005R0. (C) Candidate spherules (white arrows) within wheel scuff, ranging from 225 to 780 μm in diameter. Detail of image 0058MH0032000020R0. (D) Candidate spherules (white arrows) and a possible ellipsoid (black arrow) that range from 200 to 624 μm in diameter within a scoop location at the Rocknest sand shadow. Detail of image 0067MH0079000007R0. (E–H) Details of spherule morphology: (E) highly spherical, reflective grain; 375 μm in diameter; (F) slightly ovoid, reflective grain; 280 μm long dimension; (G) highly ovoid, reflective grain; 500 μm long dimension; (H) Smallest candidate spherule from sieved sediment deposited on Curiosity's observation tray; 106 μm in diameter, from image OO95MH013100100C0. Scale bars are 1 cm in A and B, 5 mm in C and D, and 500 μm in E–H.

et al., 2013). The MAHLI O-tray investigation of sieved sediment records a small population of possible impact spherules <100 μm in diameter (Minitti et al., 2013). Candidate impact spherules range in color from white to gray to black, but in all cases preserve a highly reflective, glassy surface, suggesting little dissolution or devitrification of the original glass. A few highly spherical grains, however, occur that are considerably dustier than candidate spherules, suggesting a higher surface roughness, or, potentially a lapilli coating. Spherules also appear to be embedded in sandstone in images of the Gillespie Lake member (Fig. 17).

Identifying the origin of highly spheroidal, yet non-reflective grains is substantially more difficult; they could represent detrital sedimentary grains, small concretions, or impact-related lapilli. Production of highly spherical particles by fluvial activity, in contrast to surface tension in a melt, is unlikely due to the polymineralic makeup of the rounded clasts as observed in ChemCam observations (Meslin et al., 2013; Cousin et al., 2015). The paucity of other fluidal morphologies, such as elongate dumbbells or teardrops, within the sand-sized fraction is surprising, but may very well be associated with the differential behavior of non-spheroidal grain morphologies during processes of aeolian grain transport (i.e., saltation-induced creep; Jerolmack et al. (2006), Minitti et al. (2013)). Lapilli, of impact or volcanic origin, are a distinct possibility for the spheroidal 'dustier" grains. Uniquely identifying lapilli would require a polished section to see either multiple layers (traditional lapilli) or a surface aggregate (armored lapilli). Melt particles and lapilli are also formed in volcanic eruptions, so their presence is not definitive evidence of an impact. However, at Gale there is no evidence of a relatively recent nearby eruption that would deposit such materials in the surficial regolith (Anderson and Bell, 2010). The pristine appearance of candidate spherules could also indicate a lack of water since their formation. Thus far, probable impact spherules have been identified in disturbed soils and drifts, as well as sediments, suggesting substantial remobilization of distal ejecta at the surface of Mars.

Could the sub-spherical outcropping particles called concretions (Fralick et al., 2012) be related to impact processes? Concretions as observed at Meridiani by the Opportunity rover are sub-spherical in shape, do not have the smooth surfaces of the glassy looking particles described here at Gale, and are considered most likely to be diagenetic in origin (Fralick et al., 2012). Particles called concretions have also been observed as blebs outcropping in the John Klein area (Sols 163–198) of the first drilling in Yellowknife Bay (Stack et al., 2013b), but these sub-spherical, rough surfaced particles are very different from the putative impact spherules, and are not likely to be impactites.

## 11. Discussion

The formation of Gale crater in the late Noachian to early Hesperian created the environment in which the materials investigated by Curiosity were deposited and subsequently impacted creating a population of small craters in the areas investigated. The small impact crater-forms (<150 m diameter) on the surface of Bradbury Rise could be primary impact craters due to the impact of meteorites, or secondary craters due to the impact of ejecta from craters outside of Gale. No craters less than 0.6 m in diameter have been observed, presumably due to atmospheric deceleration, but also to resurfacing. Crater modification in the areas explored by Curiosity can be explained by aeolian processes, with no evidence of the effects of flowing water. The absence of meteorites associated with the craters is not surprising, as terrestrial experience suggests that meteorites are usually embedded into the floors of the craters and the small fragments would be hard to identify on Mars. Secondary craters formed by ejecta from larger craters should be asymmetrical due to oblique impact, and relatively shallow, but there is little evidence for the presence of these along the rover traverse as the observed craters, however, are all generally circular as seen in vertically projected images from the rover or in HiRISE images.

Distal ejecta blocks, are likely to be represented among the float rocks documented and analyzed by ChemCam on Bradbury Rise, and they could, in part, represent a lag of erosion resistant crystalline blocks from distal sources. Sources of materials from the surrounding terrains can include materials north and south of the dichotomy boundary, the exposures of Noachian crust in the crater rim, and the sediments within Gale. In addition, the presence of paleo-channels buried by Gale ejecta suggests that early sediments may have also been present in the region. Possible candidate craters that could be the source of blocks observed by Curiosity are shown in Fig. 1B. The closest sizable crater is 4 km in diameter, and is located 15 km to the west of the landing site. Although this crater is not very fresh, it would have produced

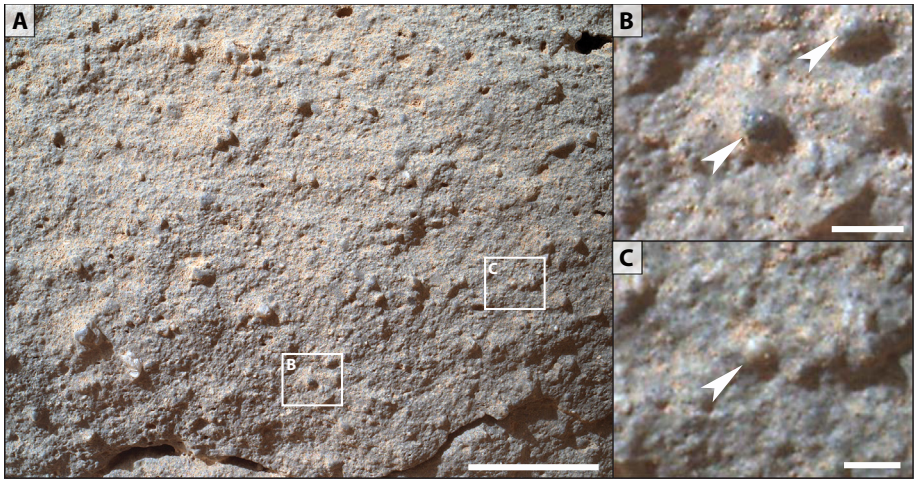


**Fig. 17.** Possible in situ impact generated spherules within lithified rock in Yellowknife Bay. (A) Best-focus Mahli Z-stack of Gillespie Lake, a highly resistant bed that overlies fine-grained, clay-rich strata of Yellowknife Bay; note a wide variety of coarse-grained components within Gillespie Lake. White boxes denote images B and C. (B) Two potential impact spherules, defined by their sphericity and their glassy, reflective surfaces. Protrusion of these spheroidal features from the wind-abraded outcrop also suggests a hardness greater than the surrounding grains. Dark gray spheroid is ~440 μm in diameter; medium gray spheroid is ~375 μm in diameter. (C) Potential impact spherule; pale gray spheroid is ~530 μm in diameter. Image 0132MH0163000010R0, with a resolution of 31.2 μm/pixel. Scale bars are 1 cm in A, and 1 mm in B and C.

substantial amounts of distal ejecta, impact spherules and impact melts. Further from the landing site, but within 3.5 crater diameters to the north east, is a prominent 23 km diameter crater, the size of the Nördlinger Ries Crater in Germany, which is younger than Gale, with a well preserved ejecta blanket. The MSL landing site area was undoubtedly affected greatly by the distal deposits from this crater and the associated blast effects. The crater is probably too far for any significant morphological effects on the basement at the landing site. However, it is completely unknown when the crater formed relative to the age of the deposits visited by Curiosity during the first 364 Sols.

Assuming the craters in the vicinity of Gale crater formed by high velocity impacts, there should be substantial amounts of materials produced by shock or melting (e.g. Schultz and Mustard (2004), and Supplement). The search for impactites, including shatter cones, shocked rocks, impact melts, spherules and lapilli, which are common indicators of impact, has only revealed a few possible examples. The smooth round spherules observed in the Rocknest drift are the most convincing evidence of materials probably associated with relatively recent impact cratering events. The surface investigations by Curiosity provide another opportunity to search for evidence for processes and materials related to impact that could be important on the surface. One example includes the coupling of the atmosphere with incoming bolides, as may have happened at Meteor Crater in Arizona that led to the scattering of iron meteorite fragments across the area (Melosh and Collins, 2005). The descending mass of hot vapor due to disintegration of a bolide during entry into the atmosphere can lead to an air burst that impacts the surface with substantial kinetic energy and high temperatures, and even melt the surface (Boslough and Crawford, 2008). On Mars, relatively small bolides can produce airbursts that reach the surface (Boslough and Crawford, 2008). However, layered impact melts from such a process have not yet been identified, possibly due to the ongoing erosion of the area.

Future remote sensing studies have the potential to identify the presence of glass from impact melts, tektites and pyroclastics, which could also allow for an improved search for these materials with Curiosity. Interestingly, a recent laboratory study (Souchon et al., 2011) has shown that natural granular surface samples comprising fresh glass or monocrystals in a high proportion are extremely forward-scattering with narrow scattering lobes. A similar photometric behavior has been previously found for a few "gray rock" samples using Pancam in situ data (Johnson et al., 2006), as well as for very glassy lunar regolith simulants (Johnson et al., 2008).

There is another phenomena, for which evidence might exist at Gale, which is the effect of oblique impacts, like Hale crater, and impact wind blast scouring from craters greater than 10 km in diameter (Schultz and Wrobel, 2012; Schultz et al., 2013). This phenomenon has been observed to form streaks around fresh craters on Mars that can extend more than 500 km from the parent crater, and may have distributed impact melt over wide areas. Some of the outcrops and blocks observed by Curiosity have a lineated surface texture (e.g. Fig. 9D and F), which could possibly be due to such events in the past. Larger scale geomorphic effects on the surface could mimic the effects of prevailing winds, and provide an additional reason for future mapping of the pattern of erosion on the surface.

No evidence of the materials or processes associated with the energetic formation of Gale itself was observed by Curiosity. Schwenzer et al. (2012) calculated that Gale had ~3600 $m^3$ of impact melt, but impact melts and impact breccias were not observed in the area studied by Curiosity, and are probably buried by the later post-impact fluvial deposits. Uplifted basement rocks that would have provided an additional substantial heat source do not seem to be evident at the surface. Hydrothermal processes are common in large terrestrial craters (Kirsimäe and Osinski, 2013). The case for the possible effects of hydrothermal processes in martian crater rim and lake deposits was laid out by Newsom et al. (1996) and Newsom (2010) and modeled by Abramov and Kring (2005). Even in the absence of visible evidence for these heat sources, there is potential in Gale for identifying post-impact hydrothermal effects in the form of alteration materials or mobile element transport that can be linked to the effects of a post-impact hydrothermal system. The maximum predicted lifetime of hydrothermal activity at Gale is limited to the $<10^6$ years immediately after crater formation (e.g., Newsom et al., 1996; Schwenzer et al., 2012), thus early post-impact processes could potentially have affected some of the fluvial or lacustrine deposits in the crater.

A possible martian example with similarities to Gale is the well-studied alluvial fan in the Late Hesperian Majuro crater in NE Hellas region. This fan is derived from the crater rim like the Peace Vallis fan, and displays a lower section with a high thermal inertia on which Fe/Mg phyllosilicates were detected and interpreted to be hydrothermal in origin (Mangold et al., 2012c). However, at Gale, there is no evidence of altered material that may have been transported from the crater rim, including cobbles with alteration veins or other evidence of shock, has been found in the fluvial deposits at Gale. The discovery of abundant phyllosilicates in the Sheepbed drill samples analyzed by the ChemMin X-ray diffraction instrument (Vaniman et al., 2013) raises the question of whether the clays were derived by alteration of the crater rim materials by hydrothermal processes (Newsom et al., 2001; Newsom, 2005; Ehlmann et al., 2011, 2013). However, the alteration minerals identified in the Sheepbed drill samples form at low-temperature (e.g. McLennan et al., 2014; Bridges et al., 2014), and the lack of chemical fractionations of elements expected for alteration has led to a model for the in situ (diagenetic) alteration of the Sheepbed mudstones (McLennan et al., 2014). The lacustrine deposits of the Sheepbed mudstone and Gillespie sandstone that are part of the bright fractured materials found in Yellowknife Bay in the Glenelg area (e.g. Grotzinger et al. (2013) and Figs. 1 and 6) were also examined in several other studies relevant to the question of impact related hydrothermal processes in impact crater lakes. On the Earth, chemical signatures of hydrothermal processes, including enrichments of Li and Ba, have been observed in the lake sediments and underlying impactites in the Yaxcopoil – 1 drill core in the 180–200 km diameter Chicxulub impact crater (Hecht et al., 2004; Zürcher and Kring, 2004; Rowe et al., 2004; Newsom et al., 2006). However, the lack of evidence for hydrothermal enrichments in the Sheepbed and Gillespie mudstone and sandstone argues against an early post Gale-impact nature of the lake in which these deposits formed. For example, lithium, which is high in terrestrial hydrothermal fluids (Newsom et al., 1999), is low in the clay-bearing materials making up the Sheepbed member of the Yellowknife Bay formation, arguing against a substantial hydrothermal input (Ollila et al., 2014; McLennan et al., 2014). Otherwise, only a few small hints of enrichments of lithium in some spots in the Bathurst_Inlet outcrop and the Rocknest_3 outcrop have been observed during the first 363 Sols (Ollila et al., 2014). There may be some evidence for hydrothermal fluids from enrichments of Mn that have been documented in what appear to be exposed fracture fills; however, these fills crosscut and therefore postdate the Gale sediments and the origin of the fluids that concentrated and deposited Mn here are as of yet unknown (Lanza et al., 2014).

A survey of impact crater depth diameters near the Curiosity traverse and an exposure age on the Sheepbed formation (Farley et al., 2013), have been used to determine a resurfacing rate in the vicinity of 8–18 mm/Myr, roughly consistent with rate

estimates elsewhere on Mars. Detailed analysis of the evolution of the characteristics of the crater fill material as a function of crater degradation may provide additional information on the rates and geomorphic processes on the surface. In addition to crater rim erosion, the shallow craters can all be seen to be filled with aeolian deposits that often form asymmetrical deposits on the crater floors.

## 12. Conclusions

Understanding the nature of impact craters on Mars is connected to the goal of the MSL mission by their connection with the formation of habitable environments, either directly by means of hydrothermal processes, or indirectly by the formation of basins where water can form lakes. Craters also provide information on timing of deposition and erosional processes that are climate related. The original floor of Gale after its formation consisted of impact melts and fall back debris. However, the actual surface over which Curiosity has traveled reflects mainly the result of later fluvial processes, which have buried the original floor materials with sedimentary rocks. Although the sedimentary materials are likely to have originated from the crater rim, no chemical or mineralogical evidence has been definitively observed from the early hydrothermal processes that probably occurred on floor or the rim of Gale. Since the crater formed ~3.6 byr ago, additional impacts on Gale have occurred in concert with sedimentation and subsequent aeolian erosion. During the first 363 Sols of the mission, no fresh craters with evidence of freshly broken rock surfaces or impact melts were observed close to the rover, but there is a distinct variation in the preservation state of craters imaged from the rover. The oldest craters are simply shallow depressions with no blocks on the rim, and a crater fill that includes a substantial component of the coarser fraction of the regolith found outside the craters. Younger craters can have blocky rims and are deeper, and typically contain finer grained fill material, typical of aeolian and dust deposits. Otherwise impactite candidates – melts and shocked rocks are rare, with the shiny spherical particles seen in the Rocknest drift providing the most likely evidence of impact generated materials.

Analysis of impact crater abundances by Grant et al. (2014) constrain the maximum burial of the current Peace Vallis Fan surface by ~40 m since ~3.2 Ga, which leads to an average resurfacing or erosion rate of ~8–14 mm/Myr. Model dependent constraints from the exposure age data from Farley et al. (2013) and the paucity of craters <2 m in diameter observed by Curiosity are plausibly within an order of magnitude of this rate. This rate is substantially greater than the resurfacing rate that can be ascribed to impact cratering alone, and is consistent with a large role for aeolian erosion and deposition. In addition, the age and erosion rate from the cratering data of Grant et al. (2014) and the depth/diameter data for craters in the vicinity of the landing site from this paper suggest that the area explored by Curiosity was not deeply buried by materials equivalent to those exposed on Mt. Sharp (e.g. Kite et al., 2013), at least since the last episodes of fan formation in Gale. However, there is a large period of time between the formation of the crater and the deposition of the Peace Vallis Fan when greater burial episodes were possible. In addition, the lower slopes of Mount Sharp have clearly been eroded back to some extent. The sediments of the Hummocky terrain between the Peace Vallis Fan and Mount Sharp may not be as young as the Peace Vallis Fan, thus the burial story may be different closer to Mount Sharp.

## Acknowledgments

We wish to thank the dedicated team of scientists, engineers and support personnel at JPL and the author's institutions for the creation and daily operation of the marvelous tool represented by the Curiosity rover and the orbital assets which provide context and communication for the MSL mission and science. Financial support provided by the Mars Science Laboratory Mission (NASA/JPL) and other institutional support. We also greatly appreciated the comments by several reviewers of this manuscript.

## Appendix A. Supplementary material

Supplementary data associated with this article can be found, in the online version, at http://dx.doi.org/10.1016/j.icarus.2014.10.013.

## References

Abramov, O., Kring, D.A., 2005. Impact-induced hydrothermal activity on early Mars. J. Geophys. Res. Planets 110, E12S09. http://dx.doi.org/10.1029/2005JE002453.

Anderson, R.C., Bell III, J.F., 2010. Geologic mapping and characterization of Gale Crater and implications for its potential as a Mars Science Laboratory landing site. Mars 5, 76–128. http://dx.doi.org/10.1555/mars.2010.0004.

Anderson, R., Bridges, J.C., Williams, A., Edgar, L., Ollila, A., Williams, J., Nachon, M., Mangold, N., Fisk, M., Schieber, J., Gupta, S., Dromart, G., Wiens, G., Le Mouélic, S., Forni, O., Lanza, N., Mezzacappa, A., Sautter, V., Blaney, D., Clark, B., Clegg, S., Gasnault, O., Lasue, J., Léveillé, R., Lewin, E., Lewis, K.W., Maurice, S., Newsom, H., Schwenzer, S.P., Vaniman, D., 2015. ChemCam results from the Shaler outcrop in Gale Crater, Mars. Icarus 249, 2–21.

Blake, D.F. et al., 2013. Curiosity at Gale Crater, Mars: Characterization and analysis of the Rocknest sand shadow. Science 341, 1239505. http://dx.doi.org/10.1126/science.1239505.

Boslough, M.B.E., Crawford, D.A., 2008. Low-altitude airbursts and the impact threat. Int. J. Impact Eng. 35, 1441–1448. http://dx.doi.org/10.1016/j.ijimpeng.2008.07.053.

Bridges, N.T., Laity, J.E., 2013. Fundamentals of aeolian sediment transport: Aeolian abrasion. In: Shroder, John F. (Ed.), Treatise on Geomorphology, vol. 11. Academic Press, San Diego, pp. 134–148.

Bridges, N.T., Ayoub, F., Avouac, J.-P., Leprince, S., Lucas, A., Mattson, S., 2012. Earth-like sand fluxes on Mars. Nature 485, 339–342. http://dx.doi.org/10.1038/nature11022.

Bridges, N.T. et al., 2014. The rock abrasion record at Gale Crater: MSL results from Bradbury Landing to Rocknest. J. Geophys. Res. Planets 119 (6), 1374–1389. http://dx.doi.org/10.1002/2013JE004579.

Bustard, A.L., Elliott, B.E., Spray, J.G., Thompson, L.M., 2012. Crater count mapping and regional geologic context of the area surrounding the Gale impact structure. Lunar Planet. Sci. XLIII. Abstract 2297.

Cabrol, N.A., Grin, E.A., Newsom, H.E., Landheim, R., McKay, C.P., 1999. Hydrogeologic evolution of Gale crater and its relevance to the exobiological exploration of Mars. Icarus 139, 235–245. http://dx.doi.org/10.1006/icar.1999.6099.

Calef III, F.J. et al., 2013. Geologic mapping of the Mars Science Laboratory landing ellipse. Lunar Planet. Sci. XLIX. Abstract 2511.

Chapman, M., Tanaka, K., 2002. Related magma–ice interactions: Possible origins of Chasma chaos and surface materials in Xanthe, Margaritifer, and Merdiani Terrae, Mars. Icarus 155 (2), 324–339. http://dx.doi.org/10.1038/nature11022.

Cousin, A., Meslin, P.Y., Wiens, R.C., Rapin, W., Fabre, C., Gasnault, O., Forni, O., Tokar, R., Ollila, A., Schröder, S., Lasue, J., Maurice, S., Sautter, V., Newsom, H., Vaniman, D., Le Mouélic, S., Dyar, D., Berger, G., Blaney, D., Nachon, M., Dromart, G., Lanza, N., Clark, B., Clegg, S., Goetz, G., Barraclough, B., Delapp, D., Blaney, D., Blaney, D., Blaney, D., 2015. the MSL Science Team, 2015. Compositions of coarse and fine particles in martian soils at Gale: A window into the production of soils. Icarus 249, 22–42.

Craddock, R.A., Howard, A.D., 2000. Simulated degradation of lunar impact craters and a new method for age dating farside mare deposits. J. Geophys. Res. Planets 105, 20387–20401. http://dx.doi.org/10.1029/1999JE001099.

Dietrich, W.E., Palucis, M.C., Parker, T., Rubin, D., Lewis, D., Sumner, D., 2014. Clues to the relative timing of lakes in Gale Crater. In: Eighth International Conference on Mars, #1178.

Edgett, K.S. et al., 2012. Curiosity's Mars Hand Lens Imager (MAHLI) investigation. Space Sci. Rev. 170, 259–317. http://dx.doi.org/10.1007/s11214-012-9910-4.

Ehlmann, B.L., Buz, J., 2014. Hydrology and aqueous alteration in the watershed of Gale, sharp, and knobel craters: A regional context for Curiosity's exploration. In: 45th Lunar and Planetary Science Conference, held 17-21 March, 2014 at The Woodlands, Texas. LPI Contribution No. 1777.

Ehlmann, B.L. et al., 2011. Subsurface water and clay mineral formation during the early history of Mars. Nature 479, 53–60. http://dx.doi.org/10.1038/nature10582.

Ehlmann, B.L. et al., 2013. Geochemical consequences of widespread clay mineral formation in Mars' ancient crust. Space Sci. Rev. 174, 329–364. http://dx.doi.org/10.1007/s11214-012-9930-0.

Eppes, M.C., McFadden, L.D., Scuderi, L.A., Wegmann, K.W., 2010. Cracks in desert pavement rocks: Further insights into mechanical weathering by directional insolation. Geomorphology 123, 97–108. http://dx.doi.org/10.1016/j.geomorph.2010.07.003.
Fairén, A.G. et al., 2014. A cold hydrological system in Gale crater, Mars. Planet. Space Sci. 93, 101–118. http://dx.doi.org/10.1016/j.geomorph.2010.07.003.
Farley, K.A. et al., 2013. In situ radiometric and exposure age dating of the martian surface. Science 343, 1247166. http://dx.doi.org/10.1126/science.1247166.
Fassett, C.I., 2013. Landscape evolution on the Moon: Crater degradation rates in the Copernican and Eratosthenian periods. GSA Annual Meeting, Abstract 275-3.
Fassett, C.I., Head III, J.W., 2008. The timing of martian valley network activity: Constraints from buffered crater counting. Icarus 195, 61–89. http://dx.doi.org/10.1016/j.icarus.2007.12.009.
Ferrière, L., Osinski, G.R., 2013. Shock metamorphism. In: Osinski, G.R., Pierazzo, E. (Eds.), Impact Cratering: Processes and Products, first ed. Wiley-Blackwell, New Jersey, pp. 106–124 (Chapter 8).
Fraeman, A.A. et al., 2013. A hematite-bearing layer in Gale crater, Mars: Mapping and implications for past aqueous conditions. Geology 41, 1103–1106. http://dx.doi.org/10.1130/G34613.1.
Fralick, P., Grotzinger, J., Edgar, L., 2012. Potential recognition of accretionary lapilli in distal impact deposits on Mars: A facies analog provided by the 1.85 Ga Sudbury impact deposit. In: Grotzinger, J.P., Milliken, R.E. (Eds.), Sedimentary Geology of Mars, vol. 102. SEPM Special Publication, pp. 211–227.
Glass, B.P., 1990. Tektites and microtektites: Key facts and inferences. Tectonophysics 171, 393–404.
Glass, B.P., 2002. Upper Eocene impact ejecta/spherule layers in marine sediments. Chem. Erde Geochem. 62, 173–196.
Golombek, M.P. et al., 2006a. Erosion rates at the Mars Exploration Rover landing sites and long-term climate change on Mars. J. Geophys. Res. Planets 111, E12. http://dx.doi.org/10.1029/2006JE002754.
Golombek, M.P. et al., 2006b. Geology of the Gusev cratered plains from the Spirit rover transverse. J. Geophys. Res. 111, E02S07. http://dx.doi.org/10.1029/2005JE002503.
Golombek, M. et al., 2012. Selection of the Mars Science Laboratory Landing Site. Space Sci. Rev. 170, 641–737. http://dx.doi.org/10.1007/s11214-012-9916-y.
Golombek, M., Warner, J., Ganti, V., Lamb, M., 2014. Erosion rates and Mars climate. In: Eighth International Conference on Mars #1359.
Grant, J.A., Wilson, S.A., 2011. Late alluvial fan formation in southern Margaritifer Terra, Mars. Geophys. Res. Lett. 38, L08201. http://dx.doi.org/10.1029/2011GL046844.
Grant, J.A., Wilson, S.A., Ruff, S.W., Golombek, M.P., Koestler, D.L., 2006a. Distribution of rocks on the Gusev Plains and on Husband Hill, Mars. Geophys. Res. Lett. 33, L16202. http://dx.doi.org/10.1029/2006GL026964.
Grant, J.A. et al., 2006b. Crater gradation in Gusev crater and Meridiani Planum, Mars. J. Geophys. Res. 111, E02S08. http://dx.doi.org/10.1029/2005JE002465.
Grant, J.A., Wilson, S.A., Mangold, N., Calef III, F., Grotzinger, J.P., 2014. The timing of alluvial activity in Gale crater, Mars. Geophys. Res. Lett. 41, 2013G. http://dx.doi.org/10.1002/L058909.
Grieve, R.A.F., Therriault, A.M., 2013. Impactites: Their characteristics and spatial distribution. In: Impact Cratering: Processes and Products, first ed. Wiley-Blackwell, New Jersey, pp. 90–105 (Chapter 7).
Grotzinger, J.P. et al., 2013. A habitable fluvio-lacustrine environment at Yellowknife Bay, Gale crater, Mars. Science 343, 1242777. http://dx.doi.org/10.1126/science.1242777.
Hartmann, W.K., Neukum, G., 2001. Cratering chronology and the evolution of Mars. Space Sci. Rev. 96, 165–194. http://dx.doi.org/10.1007/978-94-017-1035-0_6.
Hecht, L., Wittmann, A., Schmitt, R.-T., Stöffler, D., 2004. Composition of impact melt particles and the effect of post-impact alteration in suevitic rocks at the Yaxopoil-1 drill core, Chicxulub crater, Mexico. Meteorit. Planet. Sci. 39, 1169–1186. http://dx.doi.org/10.1111/j.1945-5100.2004.tb01135.x.
Jerolmack, D.J., Mohrig, D., Grotzinger, J.P., Fike, D.A., Watters, W.A., 2006. Spatial grain size sorting in eolian ripples and estimation of wind conditions on planetary surfaces: Application to Meridiani Planum, Mars. J. Geophys. Res. Planets 111, E12S02. http://dx.doi.org/10.1029/2005JE002544.
Johnson, J.R. et al., 2006. Spectrophotometric properties of materials observed by Pancam on the Mars Exploration Rovers: 1. Spirit. J. Geophys. Res. 111, E02S14. http://dx.doi.org/10.1029/2005JE002494.
Johnson, J.R., Grundy, W., Shepard, M.K., 2008. Spectrogoniometric measurements and models of lunar analog soils. Lunar Planet. Sci. XXXIX. Abstract 1331.
Kenkmann, T., Collins, G.S., Wünnemann, K., 2013. The modification stage of crater formation. In: Osinski, G.R., Pierazzo, E. (Eds.), Impact Cratering: Processes and Products, first ed. Wiley-Blackwell, New Jersey, pp. 60–75 (Chapter 5).
Kirk, R.L. et al., 2008. Ultrahigh resolution topographic mapping of Mars with MRO HiRISE stereo images: Meter-scale slopes of candidate Phoenix landing sites. J. Geophys. Res. 113, E00A24. http://dx.doi.org/10.1029/2007JE003000.
Kirk, R.L. et al., 2011. "Wall to wall" 1-m topographic coverage of the Mars Science Laboratory candidate landing sites. Lunar Planet. Sci. XLII. Abstract 2407.
Kirsimäe, K., Osinski, G.R., 2013. Impact induced hydrothermal activity. In: Osinski, G.R., Pierazzo, E. (Eds.), Impact Cratering: Processes and Products, first ed. Wiley-Blackwell, New Jersey, pp. 76–89 (Chapter 6).
Kite, E.S., Lewis, K.W., Lamb, M.P., Newman, C.E., Richardson, M.I., 2013. Growth and form of the mound in Gale Crater, Mars: Slope wind enhanced erosion and transport. Geology 41 (5), 543–546. http://dx.doi.org/10.1130/G33909.1.
Kumar, P.S., Head, J.W., Kring, D.A., 2010. Erosional modification and gully formation at Meteor Crater, Arizona: Insights into crater degradation processes on Mars. Icarus 208, 608–620. http://dx.doi.org/10.1016/j.icarus.2010.03.032.
Kuzmin, R.O., Greeley, R., Rafkin, S.C.R., Haberle, R.M., 2001. Wind-related modification of some small impact craters on Mars. Icarus 153, 61–70. http://dx.doi.org/10.1006/icar.2001.6654.
Laity, J.E., Bridges, N.T., 2013. Abraded systems. In: Shroder, John F. (Ed.), Treatise on Geomorphology, vol. 11. Academic Press, San Diego, pp. 269–286.
Lanza, N.L. et al., 2014. High manganese concentrations in rocks at Gale crater. Mars. Geophys. Res. Lett. 41 (2014), 5755–5763. http://dx.doi.org/10.1002/2014GL060329.
Le Deit, L., Hauber, E., Fueten, F., Pondrelli, M., Rossi, A.P., Jaumann, R., 2013. Sequence of infilling events in Gale crater, Mars: Results from morphology, stratigraphy, and mineralogy. J. Geophys. Res. Planets 118, 2439–2473. http://dx.doi.org/10.1002/2012JE004322.
Le Mouélic, S., Gasnault, O., Herkenhoff, K.E., Bridges, N.T., Langevin, Y., Mangold, N., Maurice, S., Wiens, R.C., Pinet, P., Newsom, H.E., Deen, R.G., Bell III, J.F., Johnson, J.R., Barraclough, B., Blaney, D., DeFlores, L., Maki, J.N., Malin, M.C., Perez, R., Saccoccio, M., 2015. The ChemCam remote micro-imager at Gale Crater: Review of the first year on Mars. Icarus 249, 93–107.
Maki, J. et al., 2011. The Mars Science Laboratory engineering cameras. Space Sci. Rev. 170, 77–93. http://dx.doi.org/10.1007/s11214-012-9882-4.
Malin, M.C., Edgett, K.S., 2000. Sedimentary rocks of early Mars. Science 290, 1927–1937. http://dx.doi.org/10.1126/science.290.5498.1927.
Malin, M.C. et al., 2007. Context camera investigation on board the Mars reconnaissance orbiter. J. Geophys. Res. 112, E05S04. http://dx.doi.org/10.1029/2006JE002808.
Malin, M.C. et al., 2010. The Mars Science Laboratory (MSL) Mast-mounted cameras (Mastcams) flight instruments. Lunar Planet. Sci. 41. Abstract 1123.
Mangold, N., Ansan, V., Allemand, P., Delacourt, C., Quantin, C., 2004. Evidence for precipitation on Mars from dendritic valleys in Valles Marineris area. Science 305, 78–81. http://dx.doi.org/10.1126/science.1097549.
Mangold, N., Kite, E.S., Kleinhans, M., Newsom, H., Ansan, V., Hauber, E., Kraal, E., Quantin-Nataf, C., Tanaka, K., 2012a. The origin and timing of fluvial activity at the Eberswalde crater, Mars. Icarus 220, 530–551. http://dx.doi.org/10.1016/j.icarus.2012.05.026.
Mangold, N., Adeli, S., Conway, S., Ansan, V., Langlais, B., 2012b. A chronology of early Mars climatic evolution from impact crater degradation. J. Geophys. Res. Planets 117, E04003. http://dx.doi.org/10.1029/2011JE004005.
Mangold, N., Carter, J., Poulet, F., Dehouck, E., Ansan, V., Loizeau, D., 2012c. Late Hesperian aqueous alteration at Majuro crater, Mars. Planet. Space Sci. 72, 18–30. http://dx.doi.org/10.1016/j.pss.2012.03.014.
Mangold, N., and the MSL team, 2014. Overview of the composition of sedimentary rocks along the Curiosity rover traverse. AGU fall meeting, San Francisco, Abstract P42C–03.
Maurice, S. et al., 2012. The ChemCam Instrument Suite on the Mars Science Laboratory (MSL) Rover: Science objectives and mast unit description. Space Sci. Rev. 170, 95–166. http://dx.doi.org/10.1007/s11214-012-9912-2.
McCall, G.J.H., 2001. Tektites in the Geological Record: Showers of Glass from the Sky. Geological Society, London.
McEwen, A.S., Preblich, B.S., Turtle, E.P., Artemieva, N.A., Golombek, M.P., Hurst, M., Kirk, R.L., Burr, D.M., Christensen, P.R., 2005. The rayed crater Zunil and interpretations of small impact craters on Mars. Icarus 176, 351–381. http://dx.doi.org/10.1016/j.icarus.2005.02.009.
McEwen, A.S. et al., 2007. Mars reconnaissance orbiter's High Resolution Imaging Science Experiment (HiRISE). J. Geophys. Res. 112, E05S02. http://dx.doi.org/10.1029/2005JE002605.
McKay, D.S., Heiken, G., Basu, A., Blanford, G., Simon, S., Reedy, R., Papike, J.J., 1991. The lunar regolith. In: Lunar Sourcebook, A User's Guide to the Moon. Cambridge University Press, pp. 285–356.
McLennan, S.M., Anderson, R.B., Bell III, J.F., Bridges, J.C., Calef III, F., Campbell, J.L., Clark, B.C., Clegg, S., Conrad, P., Cousin, A., Des Marais, D.J., Dromart, G., Dyar, M.D., Edgar, L.A., Ehlmann, B.L., Fabre, C., Forni, O., Gasnault, O., Gellert, R., Gordon, S., Grant, J.A., Grotzinger, J.P., Gupta, S., Herkenhoff, K.E., Hurowitz, J.A., King, P.L., Le Mouélic, S., Leshin, L.A., Léveillé, R., Lewis, K.W., Mangold, N., Maurice, S., Ming, D.W., Morris, R.V., Nachon, M., Newsom, H.E., Ollila, A.M., Perrett, G.M., Rice, M.S., Schmidt, M.E., Schwenzer, S.P., Stack, K., Stolper, E.M., Sumner, D.Y., Treiman, A.H., VanBommel, S., Vaniman, D.T., Vasavada, A., Wiens, R.C., Yingst, R.A., MSL Science Team, 2014. Elemental geochemistry of sedimentary rocks at Yellowknife Bay, Gale Crater, Mars. Science 343 (6169), 1244734. http://dx.doi.org/10.1126/science.1244734.
Melosh, H.J., Collins, G.S., 2005. Meteor Crater formed by low velocity impact. Nature 434, 157. http://dx.doi.org/10.1038/434157a.
Meresse, S., Costard, F., Mangold, N., Masson, P., Neukum, G., 2008. Formation and evolution of the chaotic terrains by subsidence and magmatism: Hydraotes Chaos, Mars. Icarus 194 (2), 487–500. http://dx.doi.org/10.1016/j.icarus.2007.10.023.
Meslin, P.-Y. et al., 2013. Soil diversity and hydration as observed by ChemCam at Gale Crater, Mars. Science 341, 1238670. http://dx.doi.org/10.1126/science.1238670.
Michael, G., 2013. Planetary surface dating from crater size–frequency distribution measurements: Multiple resurfacing episodes and differential isochron fitting. Icarus 226, 885–890. http://dx.doi.org/10.1016/j.icarus.2013.07.004.
Michael, G.G., Neukum, G., 2010. Planetary surface dating from crater size–frequency distribution measurements: Partial resurfacing events and statistical age uncertainty. Earth Planet. Sci. Lett. 294, 223–229. http://dx.doi.org/10.1016/j.epsl.2009.12.041.

Milliken, R.E., Grotzinger, J.P., Thomson, B.J., 2010. Paleoclimate of Mars as captured by the stratigraphic record in Gale Crater. Geophys. Res. Lett. 37, L04201. http://dx.doi.org/10.1029/2009GL041870.

Minitti, M.E. et al., 2013. MAHLI at the Rocknest sand shadow: Science and science-enabling activities. J. Geophys. Res. Planets 118, 2338–2360. http://dx.doi.org/10.1002/2013JE004426.

Newsom, H.E., 2005. Clays in the history of Mars. Nature 438, 570–571. http://dx.doi.org/10.1038/438570a.

Newsom, H.E., 2010. Heated lakes on Mars. In: Cabrol, N., Grin, E. (Eds.), Lakes on Mars. Elsevier, Amsterdam, pp. 91–110.

Newsom, H.E., Britelle, G.E., Crossey, L.J., Hibbitts, C.A., Kudo, A.M., 1996. Impact cratering and the formation of crater lakes on Mars. J. Geophys. Res. Planets 101, 14951–14955. http://dx.doi.org/10.1029/96JE01139.

Newsom, H.E., Goff, F., Hagerty, J.J., 1999. Mixed hydrothermal fluids and the origin of the martian soil. J. Geophys. Res. Planets 104, 8717–8728. http://dx.doi.org/10.1029/1998JE900043.

Newsom, H.E., Hagerty, J.J., Thorsos, I.E., 2001. Location and sampling of aqueous and hydrothermal deposits in martian impact craters. Astrobiology 1, 71–88. http://dx.doi.org/10.1089/153110701750137459.

Newsom, H.E., Nelson, M.J., Shearer, C.K., 2006. Mobile element analysis by secondary ion mass spectrometry (SIMS) of impactite matrix samples from the Yaxcopoil-1 drill core in the Chicxulub impact crater. Meteorit. Planet. Sci. 41, 1929–1945. http://dx.doi.org/10.1111/j.1945-5100.2006.tb00461.x.

Newsom, H.E. et al., 2013a. Regional and global context of soil and rock chemistry from ChemCam and Apxs at Gale crater. Lunar and Planet. Sci. 44. Abstract 1832.

Newsom, H.E., Hagerty, J.J., Misra, S., Wright, S.P., 2013b. Comparison of simple impact craters: Meteor Crater and Lonar Crater. In: Osinski, G.R., Pierazzo, E. (Eds.), Impact Cratering: Processes and Products, first ed. Wiley-Blackwell, New Jersey, pp. 271–289 (Chapter 18).

Ollila, A.M. et al., 2014. Trace element geochemistry (Li, Ba, Sr, and Rb) using Curiosity's ChemCam: Early results for Gale crater from Bradbury Landing Site to Rocknest. J. Geophys. Res. Planets 119 (1), 255–285. http://dx.doi.org/10.1002/2013JE004517.

Paige, D.A. et al., 2007. MER small crater statistics: Evidence against recent quasi-periodic climate variations. In: 7th Intl. Conf. on Mars, Abstract 3392.

Palucis, M. et al., 2014. The origin and evolution of the Peace Vallis fan system that drains to the Curiosity landing area, Gale crater, Mars. J. Geophys. Res. 119 (4), 705–728. http://dx.doi.org/10.1002/2013JE004583.

Pike, Richard J., 1980. Formation of complex impact craters: Evidence from Mars and other planets. Icarus 43, 1–19. http://dx.doi.org/10.1016/0019-1035(80)90083-4.

Quantin, C., Allemand, P., Delacourt, C., Dromat, G., Mangold, N., 2005. Fluvial and lacustrine activity on layered deposits in Melas Chasma, Valles Marineris, Mars. J. Geophys. Res. 110, E12S19. http://dx.doi.org/10.1029/2005JE002440.

Rowe, A.J., Coles, B.J., Morgan, J.V., Wilkinson, J.J., 2004. Chicxulub: Testing for post-impact hydrothermal input into the Tertiary ocean. Meteorit. Planet. Sci. 39, 1223–1231. http://dx.doi.org/10.1111/j.1945-5100.2004.tb01138.x.

Sautter, V. et al., 2014. Igneous mineralogy at Bradbury Rise: The first ChemCam campaign. J. Geophys. Res. 119, 30–46. http://dx.doi.org/10.1002/2013JE004472.

Schmidt, M.E. et al., 2013. Geochemical diversity in first rocks examined by the Curiosity Rover in Gale Crater: Evidence for and significance of an alkali and volatile-rich igneous source. J. Geophys. Res. Planets 119, 64–81. http://dx.doi.org/10.1002/2013JE004481.

Schröder, C. et al., 2008. Meteorites on Mars observed with the Mars Exploration Rovers. J. Geophys. Res. 113, E06S22. http://dx.doi.org/10.1029/2007JE002990.

Schultz, P.H., Mustard, J.F., 2004. Impact melts and glasses on Mars. J. Geophys. Res. 109, E01001. http://dx.doi.org/10.1029/2002JE002025.

Schultz, P.H., Wrobel, K.E., 2012. The oblique impact Hale and its consequences on Mars. J. Geophys. Res. 117, E04001. http://dx.doi.org/10.1029/2011JE003843.

Schultz, P.H., Quintana, S.N., 2013. Impact blast wind scouring on Mars. Lunar Planet. Sci. XLIV. Abstract 2697.

Schwenzer, S.P. et al., 2012. Gale Crater: Formation and post-impact hydrous environments. Planet. Space Sci. 70 (1), 84–95.

Silvestro, S. et al., 2012. Pervasive aeolian activity along rover Curiosity's traverse in Gale Crater, Mars. Geology 41, 483–486. http://dx.doi.org/10.1130/G34162.1.

Simonson, B.M., Byerly, G.R., Lowe, D.R., 2004. The early Precambrian record of large extraterrestrial impacts. In: Eriksson, P., Alterman, W., Catuneanu, O. (Eds.), The Precambrian Earth: Tempos and Events. Elsevier Publishing Corp., New York, NY, pp. 27–45.

Smit, J., 1999. The global stratigraphy of the Cretaceous–Tertiary boundary impact ejecta. Annu. Rev. Earth Planet. Sci. 27, 75–113. http://dx.doi.org/10.1146/annurev.earth.27.1.75.

Smit, J. et al., 1992. Tektite-bearing, deep-water clastic unit at the Cretaceous–Tertiary boundary in northeastern Mexico. Geology 20, 99–103. http://dx.doi.org/10.1130/0091-7613(1992.

Soderblom, L.A., 1970. A model for small-impact erosion applied to the lunar surface. J. Geophys. Res. 75, 2655–2661. http://dx.doi.org/10.1029/JB075i014p02655.

Souchon, A.L., Baratoux, D., Chevrel, S.D., Daydou, Y.H., Helfenstein, P., Kurita, K., Pinet, P.C., Shepard, M.K., 2011. An experimental study of Hapke's modeling of natural granular surface samples. Icarus 215, 313–331. http://dx.doi.org/10.1016/j.icarus.2011.06.023.

Spray, J.G., 2010. Frictional melting of planetary materials: From hypervelocity impact to earthquakes. Annu. Rev. Earth Planet. Sci. 38, 221–254. http://dx.doi.org/10.1146/annurev.earth.031208.100045.

Spray, J.G., Thompson, L.M., Biren, M.B., O'Connell-Cooper, C., 2010. The Manicouagan impact structure as a terrestrial analogue site for lunar and martian planetary science. Planet. Space Sci. 58, 538–551. http://dx.doi.org/10.1016/j.pss.2009.09.010.

Squyres, S.W. et al., 2004. The Spirit rover's Athena science investigation at Gusev crater, Mars. Science 305 (5685), 794–799. http://dx.doi.org/10.1126/science.1106171.

Stack, K.M. et al., 2013a. Using Outcrop Exposures on the Road to Yellowknife Bay to Build a Stratigraphic Column, Gale Crater, Mars. LPI Contributions, 1719, Abstract 1431.

Stack, K.M. et al. Team, 2013b. The distribution and origin of nodules and minibowls within the sheepbed member: Implications for early diagenesis in Yellowknife Bay, Gale crater, Mars. Geological Society of America, Abstracts with Programs, vol. 45, No. 7, p. 138.

Stolper, E., McSween Jr., H.Y., 1979. Petrology and origin of the shergottite meteorites. Geochim. Cosmochim. Acta 43, 1475–1498. http://dx.doi.org/10.1016/0016-7037(79)90142-X.

Stolper, E.M. et al., 2013. The petrochemistry of Jake_M: A martian mugearite. Science 341, 1239463. http://dx.doi.org/10.1126/science.1239463.

Sullivan, R. et al., 2008. Wind-driven particle mobility on Mars: Insights from Mars Exploration Rover observations at "El Dorado" and surroundings at Gusev crater. J. Geophys. Res. 113, E06S07. http://dx.doi.org/10.1029/2008JE003101.

Sumner, D.Y. et al., 2013. Preliminary geologic map of the Peace Vallis fan integrated with in-situ mosaics from the Curiosity rover, Gale crater, Mars. Lunar Planet. Sci. XLIV. Abstract 1699.

Tanaka, K.L., Robbins, S.J., Fortezzo, C.M., Skinner, J.A., Hare, T.M., 2014a. The digital global geologic map of Mars: Chronostratigraphic ages, topographic and crater morphologic characteristics, and updated resurfacing history. Planet. Space Sci. 95 (2014), 11–24. http://dx.doi.org/10.1016/j.pss.2013.03.006.

Tanaka, K.L. et al., 2014b. Geologic Map of Mars. United States Geological Survey Science Investigations Map 3292.

Therriault, A.M., Fowler, A.D., Grieve, R.A.F., 2002. The Sudbury igneous complex: A differentiated impact melt sheet. Econ. Geol. 97, 1521–1540. http://dx.doi.org/10.2113/gsecongeo.97.7.1521.

Thomson, B.J., Bridges, N.T., Milliken, R., Baldridge, A., Hook, S.J., Crowley, J.K., Marion, G.M., de Souza Filho, C.R., Brown, A.J., Weitz, C.M., 2011. Constraints on the origin and evolution of the layered mound in Gale crater, Mars using Mars Reconnaissance Orbiter data. Icarus 214, 413–432. http://dx.doi.org/10.1016/j.icarus.2011.05.002.

Tschermak, M.G., 1872. Die Meteorite von Shergotty und Gopalpur. Akademie der Wissenschaften in Wien Sitzungsberichte. Math.-Natur. Klasse 65, 122–146.

Vaniman, D.T. et al., 2013. Mineralogy of a mudstone at Yellowknife Bay, Gale crater, Mars. Science 343, 1243480. http://dx.doi.org/10.1126/science.1243480.

Vasavada, A.R., Milavec, T.J., Paige, D.A., 1993. Microcraters on Mars: Evidence for past climate variations. J. Geophys. Res. 98, 3469–3476. http://dx.doi.org/10.1029/92JE02942.

Watters, W.A., Bell III, J., Grant, J., Grotzinger, J.P., Hayes, A.G., Li, R., Squyres, S.W., Zuber, M.T., 2011. Origin of the structure and planform of small impact craters in fractured targets: Endurance Crater at Meridiani Planum, Mars. Icarus 211, 472–497. http://dx.doi.org/10.1016/j.icarus.2010.08.030.

Whiting, P.J., Dietrich, W.E., Drake, T.G., Leopold, L.B., Shreve, R.L., 1988. Bedload sheets in heterogeneous sediment. Geology 16, 105–108. http://dx.doi.org/10.1130/0091-7613(1988)016.

Williams, J.-P., Aharonson, O., Pathare, A., 2012. Modeling Small Impact Populations on Mars. EPSC Abstracts, vol. 7.

Williams, R.M.E. et al., 2013. Martian fluvial conglomerates at Gale crater. Science 340, 1068–1072. http://dx.doi.org/10.1126/science.1237317.

Yingst, R.A. et al., 2013. Characteristics of pebble- and cobble-sized clasts along the Curiosity rover traverse from Bradbury Landing to Rocknest. J. Geophys. Res. Planets 118, 2361–2380. http://dx.doi.org/10.1002/2013JE004435.

Zürcher, L., Kring, D.A., 2004. Hydrothermal alteration in the core of the Yaxcopoil-I borehole, Chicxulub impact structure, Mexico. Meteorit. Planet. Sci. 39, 1199–1221. http://dx.doi.org/10.1111/j.1945-5100.2004.tb01137.x.